

Public

Confidential

Project:	CHAMELEON RF
Project Number:	FP6/2004/IST/4-027378
Work Package:	WP2
Task:	T2.1
Deliverable:	D2.1a

Title:	Report on Modelling Methods for EM Interaction Between Compact Models of Devices
Author(s):	K.J. van der Kolk, N.P. van der Meijs, D. Ioan, G. Ciuprina, A. Stefanescu, D. Punga, D. Niculae, D. Mihalache, L.M. Silveira, J. Fernández, W. Schoenmaker, W. Schilders
Affiliation(s):	TUD, PUB-LMN, INESC-ID, MAGWEL, NXP
Date:	6-Aug-2007

Contents

1	Introduction	4
1.1	Introduction	4
1.2	Problem description	5
1.3	Overview	6
2	Electromagnetic Modelling Strategies	7
2.1	Introduction	7
2.2	The Full-Wave Regime	7
2.3	The Electro-Quasi-Static (EQS) Regime	8
2.4	The Magneto-Quasi-Static (MQS) Regime	8
2.5	The Electro-Magneto-Quasi-Static (EMQS) Regime	9
2.6	The Electro-Static (ES) Regime	9
2.7	The Magneto-Static (MS) Regime	9
2.8	The Electro-Conductive (EC) Regime	9
2.9	Second-order Potential Equations	10
2.10	Interface Conditions	13
2.11	Solution of the Potential Equations	13
2.12	The Non-Retarded Regime	15
3	Numerical Modelling	17
3.1	Introduction	17
3.2	The Boundary Element Method	17
3.2.1	Boundary Formulation	18
3.2.2	Discontinuity in the Surface Integrals of $\phi dg/dn$	19
3.2.3	Handling material-interfaces	20
3.2.4	Method of Moments	21
3.2.5	Discretization	23
3.2.6	Computation of Resistive Effects	25
3.2.7	Computation of Capacitive Effects	26
3.2.8	Computation of Inductive Effects	27
3.2.9	Passivity of the System	28
3.2.10	Diagonal Dominance	29
3.2.11	Boundary Element Acceleration Techniques	31
3.3	Finite Difference/Integrals Methods: FDM/FIT	33

3.4	Comparison of BEM and FDM/FIT	37
4	Conclusions	40
A	Miscellaneous Derivations and Formulae	42
A.1	Space-charge Distribution	42
A.2	Potential-functions and Gauge Freedom	42
A.3	The Coulomb gauge	43
A.4	The Lorenz gauge	44
A.5	Vector Identities	45
A.6	Green's Theorems	45

1 Introduction

1.1 Introduction

The Chameleon-RF project aims at developing methodologies and prototype tools for a comprehensive and highly accurate analysis of complete next-generation nanoscale functional IC blocks that will operate at RF frequencies of up to 60 GHz. Without describing the complete structure of the project, we note that it focuses on determining models in the first two of its work packages. While IC blocks generally consist of a couple of interconnected and interacting devices, the project in fact separates, in WP1 and WP2 respectively, the determination of models for the devices and for their interaction.

The devices as being considered in WP1 include both active devices and passive devices. Active devices are those that operate using the semi-conducting nature of the silicon substrate and have highly non-linear current-voltage relationships. Most representatively these are bipolar or CMOS transistors. Passive devices operate using the electromagnetic field behaviour that is most generally described by Maxwell's equations, but typically simplified sets of derived equations are adequate to describe their intended, ideal, behaviour. Representative types of passive devices are resistors, capacitors and inductors. Usually their terminal behaviour is linear.

Then, in WP2, the interaction among such devices is being studied. This interaction partly is of intended nature, typically via interconnect structures, and partly of parasitic nature, typically via unintended but unavoidable EM field coupling through the dielectric and substrate regions. Furthermore, the intended interconnect coupling is typically highly non-ideal, leading to further non-trivial parasitic modelling needs. In most cases, but certainly not in all cases, the semiconducting behaviour of parts of the integrated circuit can be ignored.

The purpose of this deliverable, being the first deliverable for WP2 and as put forward in the Chameleon-RF DOW, is to report on our methods for computing and modelling the interaction among the devices in RF IC blocks. Some of these methods (actually most of them) are more or less standard and even folklore, but some of them have been developed and/or refined specifically within the project,

As was already described in the DOW and documented to some extent in earlier deliverables such as D1.1 and D1.2, the concept of *hooks* is instrumental in achieving the project goals. Stated otherwise, the complete IC domain is being decomposed in sub-domains, each of which allows separate and in principle independent, local, modelling. The models for these sub-domains are then coupled in such a way that the overall model is representative for the complete domain. The (electrical) connection between the sub-models is formalised via our concept of hooks.

While each sub-domain allows local modelling, the modelling methods can also be specific for each sub-domain. If we consider the 'Maxwellian' domains, i.e. those domains that are governed by Maxwell's equations, depending on the material parameters and operating conditions, simplified sets of equations can be accurate enough as already suggested above. Exploiting this fact and using for each sub-domain the simplest possible modelling method that just gives enough accuracy, is in fact our main strategy to achieve the project goals. This concept of using different modelling methods is being formalised in this document as *modelling regimes*.

The Chameleon-RF project also envisages to separate modelling from simulation. That is, the goal is to produce an *equivalent electrical model* of an RF IC block to be subsequently subjected to electrical simulation which actually will produce time-domain waveforms, frequency-domain results such as Smith-charts or Bode diagrams and/or behavioural specifications such as S/N ratios. Thus, our aim is to emit models which are circuit-oriented and which thus allow simulation by tools of the SPICE family. (Note that such electrical simulation is *not* a project topic. However, processing models that are obtained using some project methods with the goal of compacting them w/o losing too much accuracy is a project topic, in WP3.)

While we noted that we will consider different modelling regimes, it is appropriate here to emphasise the distinction between the dielectric region above the substrate and the substrate itself. The dielectric region contains most of the interconnect network, while the substrate contains most of the active devices. Because of the vastly different properties of these regions, different modelling regimes will be appropriate for them, of course with vastly different trade-offs with respect to numerical methods to be used.

1.2 Problem description

Ultimately, the goal of our project is to provide a method for converting in an automated fashion a physical description of the interconnect structures in an integrated circuit design into a model which can be subsequently reduced in a post processing step, and finally simulated using appropriate simulation tools. As input for our algorithm, it would suffice to have a description of the wafer masks used in the fabrication of the design, since from these masks (and a small amount of extra process information) it is possible in principle to accurately compute the final physical geometries. However, we will not delve into this much detail and we will simply assume that the input consists of a description of the required physical quantities, which are expected to be obtained after fabrication.

As input to our method, we thus need

- A geometric description of the metal interconnect structures. Since interconnect on integrated circuits is layered, we may use *masks* as a data-structure to represent the vertical projection of the interconnect-geometry, and we may use a separate technology-description to describe the vertical dimensions of the metal layer-stack. This is how extraction-tools commonly work. Vias, i.e., interconnections from one layer to another, can also be modelled in this framework.
- A description of the dielectric layers above the substrate. For each layer, we need its physical height, and its permittivity. We assume for simplicity that the dielectrics are stratified, i.e., the top of each dielectric layer is a perfect horizontal plane.
- A description of the substrate doping profile, or rather conductivity profile, since we will not model semiconductor diffusion effects. We assume that the conductivity does not change continuously as we go into the substrate, but we assume that the material is stratified, i.e., we assume that the substrate is divided into

layers of constant conductivity. For each layer, we thus need its physical height, and its conductivity.

- A description of the horizontal extents of the design, i.e., the location of the saw-lane on the die. This information is necessary to model sidewall-effects. If the saw-lane is sufficiently far from the actual circuit-design, then these effects may be neglected.

The result of our method is a passive circuit-model which is suitable for simulation in circuit-simulation tools such as SPICE. The property of passivity is necessary, since it allows us to join models without losing the property of stability. Thus, when we connect our passive device-models to the interconnect models developed in this deliverable, stability is preserved.

1.3 Overview

This deliverable is structured as follows. In the next chapter, we will discuss modelling strategies at the level of the fundamental electromagnetic equations. Of course, even at the electromagnetic level, we must choose the simplest model that is still capable of describing the required effects. We will simplify Maxwell's equations using the notion of "regimes", and show what regimes are applicable under what circumstances. We will also show how the regimes are modelled using potential-equations, and how these differential equations may be turned into integral-equations, which are more suitable for discrete solution by means of the boundary element technique.

Next, we will take a close look at the numerical modelling of the electromagnetic regimes. Two discretization techniques will be reviewed, namely the boundary element method (BEM) and a method based on the Finite Difference Method and Finite Integration Technique (FDM/FIT). The advantages and drawbacks of both methods will be discussed. We will further look at the properties of the matrices resulting from the BEM method, and see under what circumstances stable systems are obtained. The modelling of resistive, capacitive and inductive effects will be discussed, and the similarities between the modelling approaches will be highlighted. An important conclusion will be that for inductive modelling, it will not be possible to perform simplification of the models by simply truncating elements in the corresponding matrices to zero. Such techniques are commonly used for resistive and capacitive models, but do not *provably* work for arbitrarily oriented inductive filaments (whether the truncated models are passive and/or stable in general is still an open problem).

2 Electromagnetic Modelling Strategies

2.1 Introduction

The electromagnetic environment which we will model is governed by Maxwell's equations, to be reviewed shortly. The model imposed by these equations, however, is too detailed for our purposes. In order to simplify the model, and hence reduce the overall extraction time and to reduce a priori the complexity of the resulting circuit models themselves, we will make simplifying assumptions. Several strategies are possible in this respect, and we will give an account of some of them in this chapter.

At the level of the electromagnetic equations, each simplification-strategy is associated with an electromagnetic “regime”, i.e., each regime imposes a set of conditions on Maxwell's fundamental equations. These conditions, of course, should be applied only when they are reasonable for a certain problem, and thus a regime may be valid only for a certain range of problems. On the other hand, given one particular electromagnetic problem, several regimes may be imposed simultaneously, each in a different part of the problem domain.

2.2 The Full-Wave Regime

The electromagnetic field in any media is described by the macroscopic Maxwell's equations¹:

$$\nabla \times \mathbf{E} = -\frac{\partial \mathbf{B}}{\partial t}, \quad (\text{Faraday's law}) \quad (2.1)$$

$$\nabla \times \mathbf{H} = \mathbf{J} + \frac{\partial \mathbf{D}}{\partial t}. \quad (\text{Ampere's law}) \quad (2.2)$$

In linear media, we have the constitutive relations

$$\mathbf{B} = \mu \mathbf{H}, \quad (2.3)$$

$$\mathbf{D} = \epsilon \mathbf{E}, \quad (2.4)$$

$$\mathbf{J} = \sigma \mathbf{E}. \quad (2.5)$$

From these relations, and by taking the divergence of (2.1) and (2.2), we find that

$$\nabla \cdot \mathbf{B} = 0, \quad (\text{Gauss's law for magnetics}) \quad (2.6)$$

$$\nabla \cdot \mathbf{D} = \rho, \quad (\text{Gauss's law}) \quad (2.7)$$

where ρ is the space charge. The last equation results from the fact that charge is a conserved quantity, and it can be obtained by taking the divergence of (2.2) (noting that the divergence of any curl is zero) and by integrating over an arbitrary volume, and then using the divergence theorem. Although the law of charge conservation is thus described completely by (2.2) and (2.7), it is often made explicit by writing

$$\nabla \cdot \mathbf{J} = -\frac{\partial \rho}{\partial t}. \quad (2.8)$$

¹The second equation is labelled “Ampere's law”, but it is actually the generalised Ampere's law, i.e., it includes the dependence on the displacement current.

The permeability and permittivity are written, respectively, as

$$\mu = \mu_0 \mu_r \quad (2.9)$$

$$\epsilon = \epsilon_0 \epsilon_r. \quad (2.10)$$

For our application, we may assume $\mu_r = 1$. The permittivity ϵ is variable over the domain of interest. Of course, if we decompose the domain such that transitions of ϵ occur only at the boundary of each subdomain, then ϵ can be taken constant inside the new domain. The same holds for σ .

Without a particular restriction for the material constants σ , μ and ϵ , Maxwell's equations describe the general case, i.e., the full-wave regime (FW). The interactions can, in this case, propagate with a finite speed $v < 1/\sqrt{\mu\epsilon}$, see [22].

2.3 The Electro-Quasi-Static (EQS) Regime

In the electro-quasi-static (EQS) regime, the materials are characterised by σ and ϵ only. All effects of the magnetic field are being neglected (\mathbf{H} plays no role), and we may assume $\mu = 0$. Hence, Maxwell's equations (Section 2.2) can be simplified to

$$\nabla \times \mathbf{E} = \mathbf{0}, \quad (2.11)$$

$$\nabla \cdot \left(\mathbf{J} + \frac{\partial \mathbf{D}}{\partial t} \right) = 0, \quad (2.12)$$

$$\nabla \cdot \mathbf{D} = \rho, \quad (2.13)$$

$$\mathbf{D} = \epsilon \mathbf{E}, \quad (2.14)$$

$$\mathbf{J} = \sigma \mathbf{E}. \quad (2.15)$$

These equations describe the capacitive and conductive effects. The transformation of these equations to the constitutive capacitive and conductive relations in a circuit-theoretical form will be detailed later. Note that the EQS regime has been applied (in an exclusive way) in many layout-to-circuit extraction tools which do not take inductive effects into account.

2.4 The Magneto-Quasi-Static (MQS) Regime

In the magneto-quasi-static (MQS) regime, the materials are characterised by σ and μ only. Capacitive effects are neglected, and this is may be modelled by assuming $\epsilon = 0$ in Maxwell's equations. Hence, we obtain the following set of equations:

$$\nabla \times \mathbf{E} = -\frac{\partial \mathbf{B}}{\partial t}, \quad (2.16)$$

$$\Rightarrow \nabla \cdot \mathbf{B} = 0, \quad (2.17)$$

$$\nabla \times \mathbf{H} = \mathbf{J}, \quad (2.18)$$

$$\mathbf{B} = \mu \mathbf{H}, \quad (2.19)$$

$$\mathbf{J} = \sigma \mathbf{E}. \quad (2.20)$$

This regime describes all inductive effects (self-inductance, mutual inductance, skin effect, eddy currents), as well as conduction. The MQS regime in itself is not very interesting for VLSI applications, since it neglects the capacitive effects (which are most important in our class of problems). However, the MQS regime can be augmented with, e.g., the EQS regime as we will see next.

2.5 The Electro-Magneto-Quasi-Static (EMQS) Regime

There is also a special field regime, called the electro-magneto-quasi-static (EMQS) regime. In this case, in the highly conductive part of the computational domain (e.g. in the metallic conductors) the field is considered MQS, and in the remainder (e.g. in the insulating dielectrics) it is considered to be EQS. Despite this hybrid approach, the EMQS regime is able to model the propagation along the interface between the EQS and MQS subdomains.

Note that in our view or definition, the EMQS regime applies two different sets of equations (MQS and EQS), which are mutually exclusive in each part of the domain. This stands in contrast with the Non-Retarded regime (to be discussed later), which applies a mixture of similar equations to the complete domain.

2.6 The Electro-Static (ES) Regime

The simplest electromagnetical regimes are the static ones. The electro-static (ES) regime describes only the capacitive effects. In this case, only the material constant ϵ is of importance.

The governing equations result from Maxwell's equations by setting $\partial/\partial t = 0$, but retaining charge conservation. Hence,

$$\nabla \times \mathbf{E} = \mathbf{0}, \quad (2.21)$$

$$\nabla \cdot \mathbf{D} = \rho, \quad (2.22)$$

$$\mathbf{D} = \epsilon \mathbf{E}. \quad (2.23)$$

Again, this regime, by itself, is not very interesting. We use the definition of this regime here so that we can refer to it later when we combine different regimes. This is also the case for the following static regimes.

2.7 The Magneto-Static (MS) Regime

The magneto-static (MS) regime describes only the magnetic/inductive effects. The material constant μ is sufficient to describe the behaviour of the materials in this case. The governing equations are:

$$\nabla \times \mathbf{H} = \mathbf{0}, \quad (2.24)$$

$$\nabla \cdot \mathbf{B} = 0, \quad (2.25)$$

$$\mathbf{B} = \mu \mathbf{H}. \quad (2.26)$$

2.8 The Electro-Conductive (EC) Regime

The Electro-Conductive (EC) regime describes only the conductive effects, where σ is sufficient to describe the material behaviour. The corresponding equations are:

$$\nabla \times \mathbf{E} = \mathbf{0}, \quad (2.27)$$

$$\nabla \cdot \mathbf{J} = 0, \quad (2.28)$$

$$\mathbf{J} = \sigma \mathbf{E}. \quad (2.29)$$

2.9 Second-order Potential Equations

In all static regimes the electric field strength has a zero curl, therefore it may be expressed as a gradient of a scalar potential. Let us consider the Electro-Static (ES) regime. The electric scalar potential ϕ is defined by:

$$\mathbf{E} = -\nabla\phi. \quad (2.30)$$

Combining (2.22) with (2.23), we obtain a generalised Poisson equation

$$\nabla \cdot \epsilon \nabla \phi = -\rho, \quad (2.31)$$

or a generalised Laplace equation,

$$\nabla \cdot \epsilon \nabla \phi = 0, \quad (2.32)$$

when $\rho = 0$. Moreover, in a homogeneous sub-domain, where ϵ is constant, the electric potential ϕ is the solution of the Laplace equation

$$\Delta\phi = 0. \quad (2.33)$$

Note that in any homogeneous domain no space-charge can exist (see also Section A.1), and this explains the zero r.h.s. in the above equation. Free or bound charge will only occur at the interface between two different types of material, and therefore the space-charge-density ρ in (2.31) is usually interpreted in a distributional sense, i.e., the space-charge-density is actually zero everywhere, except at the interface, where it is infinite. A volume integral around the interface, however, will yield the (finite) amount of charge present at the interface.

In the Electro-Conductive (EC) regime, the electric potential is defined as in (2.30), since, again, the curl of the electric field is zero.

Equation (2.28) is valid for the interior of the domain. At the boundary, where current may be injected (or ejected), this equation obviously does not hold. Therefore, we write it as

$$\nabla \cdot \mathbf{J} = -I_{\text{in}}, \quad (2.34)$$

where I_{in} is the amount of current injected per unit volume (units: $[A/m^3]$). Note that this equation is in fact equivalent to (2.8). Combining the above expressions with Ohm's law (2.29), we obtain a generalised Poisson equation,

$$\nabla \cdot \sigma \nabla \phi = -I_{\text{in}}. \quad (2.35)$$

For homogeneous domains (σ constant), this translates into a regular Poisson equation,

$$\Delta\phi = -\frac{I_{\text{in}}}{\sigma}. \quad (2.36)$$

Note that I_{in} is a space-current-density, i.e., an amount of current injected per unit space. Since charge cannot be created, this density is to be interpreted in a distributional sense, i.e., the space-current-density is zero everywhere, except (for example)

at some surface, where it is infinite; any volume-integral around the surface will actually yield the finite current which is injected into the domain.

In the Magneto-Static (MS) regime, the magnetic scalar potential ϕ_m is defined similarly as above, but this time the curl of the magnetic field is zero, see (2.24). Thus, we write

$$\mathbf{H} = -\nabla\phi_m. \quad (2.37)$$

As above, we obtain the generalized Laplace equation

$$\nabla \cdot \mu \nabla \phi_m = 0, \quad (2.38)$$

or

$$\Delta\phi_m = 0 \quad (2.39)$$

in domains with homogeneous magnetic properties (as will be generally the case in any integrated circuit).

In conclusion, all three static fields satisfy a similar PDE of the second order and of elliptic kind, and thus from a mathematical point of view, all cases are identical.

The Electro-Quasi-Static (EQS) regime allows a similar definition of the electric potential as above. See equations (2.11)...(2.15). However, here ϕ is time-dependent. In the frequency-domain (with the complex frequency variable $s = j\omega$), the charge-conservation equation (2.12) becomes

$$\nabla \cdot (\mathbf{J} + s\mathbf{D}) = 0, \quad (2.40)$$

or,

$$\nabla \cdot (\sigma + s\epsilon)\mathbf{E} = 0, \quad (2.41)$$

or, formulated in terms of the scalar electric potential,

$$\nabla \cdot [(\sigma + s\epsilon)\nabla\phi] = 0, \quad (2.42)$$

which in an homogeneous domain reduces again to the Laplace equation $\Delta\phi = 0$.

In the Magneto-Quasi-Static (MQS) regime, the magnetic flux density has zero divergence, and therefore it is preferable to use the magnetic vector potential \mathbf{A} , defined by

$$\mathbf{B} = \nabla \times \mathbf{A}. \quad (2.43)$$

However, the above definition leaves the divergence of \mathbf{A} still free. See also Section A.2. Here, we choose

$$\nabla \cdot \mathbf{A} = 0, \quad (2.44)$$

i.e., the Coulomb gauge, see (A.13). Thus, we have the following relation

$$\mathbf{E} = -(\nabla\phi + s\mathbf{A}), \quad (2.45)$$

which is identical to (A.9). Combining (2.45), (2.19), (2.18), and (2.20), we find

$$\nabla \times \frac{1}{\mu} \nabla \times \mathbf{A} + s\sigma \mathbf{A} + \sigma \nabla \phi = 0, \quad (2.46)$$

$$\nabla \cdot (\sigma \nabla \phi) + s \nabla \cdot (\sigma \mathbf{A}) = 0, \quad (2.47)$$

where the latter equation was derived by taking the divergence of the former. In homogeneous domains (where μ and σ are constant), we can rewrite the above pair of equations as

$$-\Delta \mathbf{A} + s\mu\sigma \mathbf{A} + \mu\sigma \nabla \phi = 0, \quad (2.48)$$

$$\Delta \phi = 0. \quad (2.49)$$

Note that the former equation is of the Helmholtz type, whereas the latter is of the Laplace type. A simpler Helmholtz equation is obtained for the electric field $\mathbf{E} = \mathbf{J}/\sigma$, by the following series of steps

$$\nabla \times \nabla \times \mathbf{E} = -s \nabla \times \mathbf{B} = -s\mu \nabla \times \mathbf{H} = -s\mu\sigma \mathbf{E}. \quad (2.50)$$

In homogeneous domains, there is no accumulation of space charge, and thus $\nabla \cdot \mathbf{E}$ (A.3) holds. Then, we can use the vector identity (A.23) with $\mathbf{F} \rightarrow \mathbf{E}$ to obtain

$$-\Delta \mathbf{E} + s\mu\sigma \mathbf{E} = 0. \quad (2.51)$$

In the full-wave (FW) regime, as explained in Section A.4, we may use the Lorenz-gauge (A.20) to obtain a decoupled pair of Helmholtz equations for the scalar and vector potential:

$$\Delta \phi - \frac{s^2}{c^2} \phi = -\frac{\rho}{\epsilon}, \quad (2.52)$$

$$\Delta \mathbf{A} - \frac{s^2}{c^2} \mathbf{A} = -\mu \mathbf{J}, \quad (2.53)$$

with

$$c = 1/\sqrt{\mu\epsilon} \quad (2.54)$$

the propagation speed of electromagnetic waves in the particular medium.

It should be remarked that the above set of equations do not model any conductive effects. That is, the current density is an explicit part of the equations, and we have not used (2.5). The occurrence of the current density can be eliminated by choosing the gauge-condition

$$\nabla \cdot \mathbf{A} = -\mu(\sigma + s\epsilon)\phi, \quad (2.55)$$

so that

$$\Delta \phi - \gamma^2 \phi = -\frac{\rho}{\epsilon}, \quad (2.56)$$

$$\Delta \mathbf{A} - \gamma^2 \mathbf{A} = \mathbf{0}, \quad (2.57)$$

where

$$\gamma^2 = s\mu(\sigma + s\epsilon). \quad (2.58)$$

It is noted that setting $\sigma = 0$ in (2.55) brings us back at the Lorenz-gauge (A.20).

2.10 Interface Conditions

From Maxwell's equations, and by using the divergence theorem, and Stokes' theorem, we can formulate conditions that must hold at the interface between any two materials, see [8].

$$\mathbf{n} \times (\mathbf{H}_2 - \mathbf{H}_1) = \mathbf{J}_{\text{surface}} (= 0), \quad (2.59)$$

$$\mathbf{n} \times (\mathbf{E}_2 - \mathbf{E}_1) = 0, \quad (2.60)$$

$$\mathbf{n} \cdot (\mathbf{D}_2 - \mathbf{D}_1) = \rho_{\text{surface}}, \quad (2.61)$$

$$\mathbf{n} \cdot (\mathbf{B}_2 - \mathbf{B}_1) = 0 \quad (2.62)$$

Note that $\mathbf{J}_{\text{surface}}$ is a surface current (units: $[A/m]$), and is usually zero, since such currents can only theoretically exist when the conductivity is infinitely large. On the other hand, ρ_{surface} is a surface-charge (units: $[C/m^2]$), and it can physically exist. However, note that this surface-charge is free-charge, and it should not be confused with polarisation charge (which is a concept not used in our framework).

Using the condition (2.61), we see that on the interface between two dielectric layers, the potentials ϕ_1 and ϕ_2 in these layers satisfy the following relations:

$$\phi_1 = \phi_2 \quad \text{and} \quad \epsilon_2 d\phi_2/dn - \epsilon_1 d\phi_1/dn = \rho_{\text{surface}}, \quad (2.63)$$

where the potential is enforced to be continuous, since we require that the electric field remains finite. We will use the above expression when we will formulate an expression for the electromagnetic interaction in inhomogeneous domains, see Section 3.2.

2.11 Solution of the Potential Equations

In the previous section, we showed that, depending on the regime at work, we could write down a single potential equation or a set of potential equations. The potentials are, depending on the case, of scalar or of vector-type. Fortunately, the case of solving for a vectorial potential is mathematically equivalent to solving three times for a scalar potential, since

$$\Delta \mathbf{A} \equiv \begin{pmatrix} \Delta A_1 \\ \Delta A_2 \\ \Delta A_3 \end{pmatrix}. \quad (2.64)$$

See also the definition (A.23), which is essentially the source of the vectorial Laplace operator. Now, let us choose ϕ to be the unknown variable (and we may replace it by ϕ_m , or the vector-components A_1 , A_2 , etc. if required). We take the Helmholtz equation as starting point, as it covers the most general case (simply set $k = 0$ to obtain the Poisson equation). Further, we incorporate the material constant χ , which may be replaced by the permittivity ϵ , the permeability μ , or the conductivity σ , when desired. Thus, our general equation is of the form

$$(\Delta + k^2)\phi = -\varsigma/\chi, \quad (2.65)$$

where k is an arbitrary complex constant (k^2 may be negative), and ς/χ is called the source-term. For conciseness, we add the dependency on the spatial coordinate

variable $\mathbf{r} = (x, y, z)$ to the above equation.

$$(\Delta_{\mathbf{r}} + k^2)\phi(\mathbf{r}) = -\varsigma(\mathbf{r})/\chi \quad (2.66)$$

The subscript of the Laplace-operator denotes the coordinate-variable it operates upon.

Now, we define the function $g(\mathbf{r}, \mathbf{r}')$ to be the solution of the above Helmholtz equation, for the case that ς equals a point-source at the location \mathbf{r}' , and for the case that $\chi = 1$. This is implemented by means of the delta-function shifted to \mathbf{r}' . Thus,

$$(\Delta_{\mathbf{r}} + k^2)g(\mathbf{r}, \mathbf{r}') = -\delta(\mathbf{r} - \mathbf{r}'). \quad (2.67)$$

The solution g to this particular problem is called a Green's function. When the computational domain is unbounded, which we will assume here, and when we impose the boundary-condition $g \rightarrow 0$ as $|\mathbf{r} - \mathbf{r}'| \rightarrow \infty$, then the solution g is called the free-space Green's function (and also in this case the "fundamental solution of the Helmholtz operator"). The boundary-condition will make the solution physically more intuitive, and it will make the Green's function unique. Since we have set $\chi = 1$, the material constant will be left out of the Green's function in our case.

Now, to determine the 3-d fundamental solution g , assume that the point-source is located at the origin, and assume that $r > 0$. Then, from spherical symmetry, we can write

$$(\Delta + k^2)g(r) = 0, \quad (r > 0) \quad (2.68)$$

where the dependence on \mathbf{r}' has been temporarily dropped from our notation, for convenience. Now, using the spherical form of the Laplace-operator, and noting that g is a function of r only, we can rewrite the above as

$$\left(\frac{\partial^2}{\partial r^2} + k^2\right)rg(r) = 0. \quad (2.69)$$

The solution to the above equation is

$$rg(r) = Ae^{-jkr} + Be^{+jkr}, \quad (2.70)$$

and, because $r \neq 0$,

$$g(r) = A\frac{e^{-jkr}}{r} + B\frac{e^{+jkr}}{r}. \quad (2.71)$$

Because of the boundary condition $g(r \rightarrow \infty) = 0$, we have that $B = 0$ must hold. Further, we may find that $A = 1/4\pi$ by integrating (2.67) over a spherical volume around the origin, and limiting the radius of the sphere towards 0 (see [7], Section 1.3.3 for details). The resulting Green's function is

$$g(\mathbf{r}, \mathbf{r}') = \frac{e^{-jk|\mathbf{r}-\mathbf{r}'|}}{4\pi|\mathbf{r}-\mathbf{r}'|}. \quad (2.72)$$

For the case of a Laplace or Poisson equation, we have that $k = 0$ in (2.65), and thus the above definition of the Green's function degenerates into

$$g(\mathbf{r}, \mathbf{r}') = \frac{1}{4\pi|\mathbf{r}-\mathbf{r}'|}. \quad (2.73)$$

We will use the above Green's function for the Helmholtz case to solve the Helmholtz equation (2.65). First, we define

$$\mathcal{L}_r = \Delta_r + k^2, \quad (2.74)$$

thus (2.66) is written

$$\mathcal{L}_r \phi(\mathbf{r}) = -\varsigma(\mathbf{r})/\chi. \quad (2.75)$$

Now, we multiply both sides of (2.67) by $\varsigma(\mathbf{r}')$, and integrate the equation using primed coordinates throughout the domain Ω . Then, by the sifting property of the delta-function, we have that

$$\int_{\mathbf{r}' \in \Omega} [\mathcal{L}_r g(\mathbf{r}, \mathbf{r}')] \varsigma(\mathbf{r}') dr' = -\varsigma(\mathbf{r}) \quad (2.76)$$

Under certain conditions, we can take the linear operator \mathcal{L}_r outside the integral. This is justified by the fact that this operator works on unprimed coordinates \mathbf{r} , while $\varsigma(\mathbf{r}')$ depends on primed coordinates. Finally, we use (2.75), to obtain the solution

$$\phi(\mathbf{r}) = \int_{\mathbf{r}' \in \Omega} \frac{g(\mathbf{r}, \mathbf{r}')}{\chi} \varsigma(\mathbf{r}') dr'. \quad (2.77)$$

This relation is essentially equivalent to (2.65), although it is expressed in the form of a so-called integral-equation of the first kind. This form is more convenient for discretization, especially when we wish to work with "boundary elements", i.e., if we wish to discretize only the surfaces comprising the material-interfaces. The topic of discretization will be treated in more depth in the next chapter. In that chapter, we will also address the issues related to inhomogeneous materials, and we will see more clearly under what conditions the above derivation is valid.

To avoid misunderstanding, we finally note here that the separation of the vector potential into three scalar potentials (one for each direction in a Cartesian coordinate system) seems to restrict this method to Cartesian coordinates and ultimately, for numerical purposes, to equidistant regular grids. However, this is only true for the sub-domain that this approach is being applied to. It does not impair the flexibility of the overall solving technique. Different sub-domains can use different solution methods with different meshing techniques, and are only coupled via the mechanism of the hooks which was fully developed in Deliverable 1.2.

2.12 The Non-Retarded Regime

If we compare the Green's function (2.72) for the Helmholtz equation to the Green's function (2.73) for the Poisson equation, we note that there is only a difference in the numerator of both equations. By applying the inverse-Laplace transform, we see that the exponential in the numerator of the Helmholtz Green's function introduces a delay w.r.t. the Green's function for the Poisson equation.

Considering the equations (2.52) and (2.53) (which are valid for full-wave, but do not model conduction-losses), and comparing them to (2.65), we have for both the scalar and vector potentials that $k^2 = -s^2/c^2$.

Thus, (2.72) may be rewritten as

$$g(\mathbf{r}, \mathbf{r}') = \frac{e^{s\tau}}{4\pi|\mathbf{r} - \mathbf{r}'|}, \quad (2.78)$$

where

$$\tau = \frac{|\mathbf{r} - \mathbf{r}'|}{c} \quad (2.79)$$

is the introduced delay. This delay is commonly known as the *retardation*.

On a small scale, thus when $|\mathbf{r} - \mathbf{r}'|$ is small compared to the wavelength $\lambda = c/f$, the retardation τ is also small, and this forms the basis for the so-called Non-Retarded regime. In the Non-Retarded regime, we simply replace the Green's functions for the Helmholtz equations (valid in the full-wave regime) by the Green's functions for the Poisson equation. In other words, we simply set $k = 0$, or, equivalently, we set $\tau = 0$. Equations (2.52) and (2.53) thus reduce to

$$\Delta\phi = -\frac{\rho}{\epsilon}, \text{ and} \quad (2.80)$$

$$\Delta\mathbf{A} = -\mu\mathbf{J}. \quad (2.81)$$

The Non-Retarded regime, as discussed, is valid when the geometry is small w.r.t. the wavelength, say $|\mathbf{r} - \mathbf{r}'| < \lambda/10$. We note that in this regime, it is not possible to model the energy-loss due to radiation-effects. However, this loss can be considered insignificant when the above geometrical assumptions are valid.

In our case, we have that $f_{\max} = 60GHz$ and thus $\lambda_{\min}/10 = 500\mu m$. This is about the size of the largest devices to be expected on a chip, except perhaps for relatively long interconnect-structures. Thus, to a reasonable extent the approximation may be considered valid. Again we note that the equations do not model conductive losses, and thus these have to be modelled separately.

One issue regarding the Non-Retarded regime is that for the derivation of the full-wave Helmholtz equations we used the Lorenz gauge, whereas for the derivation of the Poisson equations for the Non-Retarded regime, we implicitly used the Coulomb gauge, and we ignored the displacement current in the derivation of the inductive effects (the Poisson equation for the vector potential). This means that if we choose the Lorenz gauge to hold, then our approximation consists of the omission of the retardation, whereas if we choose the Coulomb gauge to hold, then our approximation consists of the deletion of the displacement current in the magnetic case. It is not clear which gauge is more appropriate, but for the Lorenz gauge we can explain the approximation in terms of geometrical distances.

Finally, we note again, that the Non-Retarded regime is different from the EMQS regime in our definition, because the Non-Retarded regime applies both the ES and MS equations in the complete domain, whereas the EMQS regime separates the equations and lets them govern separately in different parts of the domain: EQS in subdomains with low conductivity, and MQS in subdomains with high conductivity. In the Non-Retarded regime, the field-equations are of elliptic type, whereas in the EMQS regime they are of parabolic type. Further, the EMQS regime models the conductive losses, in contrast to the Non-Retarded regime, but we will extend the Non-Retarded regime with the EC regime to solve this deficiency,

3 Numerical Modelling

3.1 Introduction

In this chapter, we will take the formulations of the electromagnetic regimes from the previous chapter and translate them into a numerical language. This means that the continuous equations are replaced by discrete ones, and since the electromagnetic problems are inherently linear, we will arrive at linear systems of equations.

There are different ways to discretize the electromagnetic equations, and each has advantages and disadvantages. The Boundary Element Method (BEM), to be discussed shortly, can be applied to explicitly compute the electromagnetic quantities at the defining surfaces of a domain only, i.e., at surfaces where the material constants change. The main advantage is clear: only a surface-discretization is needed and thus the number of unknowns in the resulting system of equations (and thus the size of the main matrix) is limited. On the other hand, the number of interactions in the resulting system turns out to be maximal, which means that the resulting matrix is dense.

The Finite Difference Method (FDM) and Finite Integration Technique (FIT) are discretization methods which follow closely the original formulation of Maxwell's equations, either in differential form (in case of FDM), or in integral form (in case of FIT). Since these methods are so closely tied to the original PDE's, they are robust in the sense that any approximations made by the discretization can be directly explained in terms of the original equations and field quantities. However, these methods require the complete domain space to be discretized, meaning that the resulting matrices may become quite large for 3D-problems, although the matrices are extremely sparse in general.

In this chapter, we will review the BEM and FDM/FIT methods, and highlight the properties needed in the remainder of the discussion. We will also see how some of the disadvantages of the BEM can be remedied, and how a compromise between both worlds can be found, although the details will be saved for the next chapter.

3.2 The Boundary Element Method

In this section we will review the Boundary Element Method (BEM). As explained, the BEM requires only the surfaces in the domain to be discretized, and hence offers the advantage of a smaller resulting linear system. In order to make the discretization, the differential equations for the electric scalar and magnetic vector potential, for the various regimes, must be cast in integral-form, as explained in the previous chapter.

Usually the BEM is applied by restricting the integrals to the surfaces of the domain and then discretizing the surfaces into individual panels. However, we will also allow elements with a three-dimensional volume. This will be useful for modelling the current-density in conducting bodies, while still adhering to the formalism imposed by the BEM.

3.2.1 Boundary Formulation

Here we will again derive an integral equation from the potential equations, just as we did in Section 2.11. However, we will now consider the case when the domain is not infinitely large. This will introduce some subtleties, but it will allow us to later treat the case of inhomogeneous domains.

Note that the integral equation (2.77) describes a relation between sources and potentials. If the sources are located only on surfaces (and are then to be interpreted in a distributional sense), then the volume-integral can be replaced by a surface-integral. In principle, we would then already have arrived at a boundary-formulation, and we will see at the end of this section that our result will correspond to this one, in case the domain is homogeneous, and infinitely large.

Consider the partial differential equation (2.66), valid over the domain Ω . Note that the associated Green's function is (2.72), so that (2.67) holds.

Now, set $u = \phi$ and $w = g$ in Green's second theorem, (A.27), and let $V = \Omega - \Omega_\delta$, and $S = \partial V$. Then,

$$\int_{S+S_\delta} [\phi(dg/dn) - g(d\phi/dn)] dS = \int_{\Omega-\Omega_\delta} [\phi\Delta g - g\Delta\phi] dV, \quad (3.1)$$

where the surface normal is outward of $\Omega - \Omega_\delta$. Now, we let Ω_δ be a sphere with radius δ , centered around \mathbf{r}' , and we take the limit $\delta \rightarrow 0$. If we look at the surface integral over S_δ , we have

$$\lim_{\delta \rightarrow 0} \int_{S_\delta} [\phi(dg/dn) - g(d\phi/dn)] dS = \lim_{\delta \rightarrow 0} \int_{S_\delta} [\phi(dg/dn)] dS,$$

where the second term vanishes since g is $O(1/\delta)$ and dS is $O(\delta^2)$ and we assume that $\nabla\phi$ is finite everywhere (!) Using Green's first theorem, (A.26), the above expression can be rewritten as

$$- \lim_{\delta \rightarrow 0} \int_{V_\delta} [\phi\Delta g + \nabla\phi \cdot \nabla g] dV,$$

where the leading minus-sign occurs because we now integrate over Ω_δ , and we must flip the normal. Using (2.67) we have,

$$\lim_{\delta \rightarrow 0} \int_{V_\delta} [\phi\delta(\mathbf{r} - \mathbf{r}') + \phi k^2 g - \nabla\phi \cdot \nabla g] dV.$$

Since dV is $O(\delta^3)$ and we assume that both ϕ and $\nabla\phi$ remain finite (!) only the first term remains, which, using the sifting property of the delta function, can be evaluated as $\phi(\mathbf{r}')$.

Now, we rewrite the volume integral of (3.1). Multiplying (2.67) by ϕ , and (2.66) by g , and subtracting, we obtain

$$\int_{\Omega-\Omega_\delta} [\phi\Delta g - g\Delta\phi] dV = \int_{\Omega-\Omega_\delta} \left[-\phi(\mathbf{r})\delta(\mathbf{r} - \mathbf{r}') + \frac{g(\mathbf{r}, \mathbf{r}')}{\chi} \zeta(\mathbf{r}) \right] dV$$

Since \mathbf{r}' is not contained in the domain $\Omega - \Omega_\delta$, the first term at the right can be dropped, and thus

$$\int_{\Omega-\Omega_\delta} [\phi\Delta g - g\Delta\phi] dV = \int_{\Omega-\Omega_\delta} \frac{g(\mathbf{r}, \mathbf{r}')}{\chi} \zeta(\mathbf{r}) dV.$$

Concluding, (3.1) can be written as

$$F\phi(\mathbf{r}') = \lim_{\delta \rightarrow 0} \int_{\Omega - \Omega_\delta} \frac{g(\mathbf{r}, \mathbf{r}')}{\chi} \varsigma(\mathbf{r}) dV - \int_S [\phi(dg/dn) - g(d\phi/dn)] dS. \quad (3.2)$$

Note that the sign of the surface integral depends on the orientation of the normal vector. In our case, the normal points outward the domain. Further, we have $F = 1$ when \mathbf{r}' is inside the domain Ω , and $F = 0$ when \mathbf{r}' is outside the domain. We will not go into the details of determining F when \mathbf{r}' is at the boundary of the domain. In that case, it turns out that $F = 1/2$ when the boundary is sufficiently smooth (which we will assume).

3.2.2 Discontinuity in the Surface Integrals of $\phi dg/dn$

Consider in the r.h.s. of Equation (3.2) the integral

$$\int_\Gamma \phi \nabla g(\mathbf{r}, \mathbf{r}') \cdot d\mathbf{\Gamma}. \quad (3.3)$$

This integral is in general not continuous as \mathbf{r}' approaches Γ from both sides. In fact, it can be derived that

$$\lim_{\mathbf{r}' \rightarrow \mathbf{r}'_s} \int_\Gamma \phi(\mathbf{r}) \nabla g(\mathbf{r}, \mathbf{r}') \cdot d\mathbf{\Gamma} = \pm \frac{\phi(\mathbf{r}'_s)}{2} + \int_\Gamma \phi(\mathbf{r}) \nabla g(\mathbf{r}, \mathbf{r}'_s) \cdot d\mathbf{\Gamma}, \quad (3.4)$$

where the upper sign (plus) occurs in case the limit is taken from the side of Γ towards which \mathbf{n} is directed, and the lower sign otherwise. Note that the above formula holds for any function ϕ , which is well-behaved around \mathbf{r}'_s (i.e., the relation between ϕ and g is not important to show this). The derivation is given, e.g., in [19], for g being the free-space Green's function, and the derivation for g being the Helmholtz Green's function is similar.

An intuitive explanation for the above equation is given now. First, we introduce a ball-shaped neighbourhood \mathcal{B}_ε of \mathbf{r}'_s , where the ball is centered at \mathbf{r}'_s , and has radius ε . We only need to show that (3.4) holds if we replace Γ by the surface $\mathcal{S}_\varepsilon = \Gamma \cap \mathcal{B}_\varepsilon$. In the limit of $\varepsilon \rightarrow 0$, under the assumption that Γ is sufficiently smooth, the surface \mathcal{S}_ε can be considered to be a flat disk \mathcal{D}_ε with centre \mathbf{r}'_s (and with associated normal oriented in the same direction as that of Γ at \mathbf{r}'_s). If we also assume that ϕ is well-behaved, then under these limiting conditions, ϕ can be considered constant, and thus it can be taken outside the integral signs, and outside the limit.

It is possible to show that for any flat disk \mathcal{D} of any radius (and \mathbf{r}'_s its centre),

$$\int_{\mathcal{D}} \nabla g(\mathbf{r}, \mathbf{r}'_s) \cdot d\mathcal{D} = 0. \quad (3.5)$$

This eliminates the rightmost integral of (3.4) under the condition $\varepsilon \rightarrow 0$. What remains, is for us to show that

$$\lim_{\mathbf{r}' \rightarrow \mathbf{r}'_s} \int_{\mathcal{D}_\varepsilon} \nabla g(\mathbf{r}, \mathbf{r}') \cdot d\mathcal{S} = \pm 1/2. \quad (3.6)$$

This equation can be shown to hold for a disk of any radius (and in fact for any flat surface containing \mathbf{r}'_s in its interior). We will not elaborate on the evaluation of this integral itself, as this is not so important, and it can be considered a more or less trivial exercise.

3.2.3 Handling material-interfaces

In the previous chapter, we mostly assumed that materials are piecewise homogeneous. We formulated the governing potential equations for the homogeneous sub-domains, but we left the interaction of the EM fields and potentials at the interfaces mostly unspecified.

In general, if we consider an inhomogeneous domain, we have an equation of the generalised Poisson form,

$$\nabla \cdot \chi \nabla \phi = -\varsigma, \quad (3.7)$$

where $\chi = \chi(\mathbf{r})$ is the material parameter. We keep the discussion abstract, thus depending on the problem, χ can be either the permittivity, or the conductivity, etc. and ϕ can be the electric scalar potential, or it can be one of the components of the magnetic vector potential, as before.

Consider now two domains Ω_1 and Ω_2 , which are nested, with closed surface Γ separating them (assume there is no other boundary, or that this boundary is at infinity, and hence unimportant). Assume that domain Ω_i has a uniform material parameter χ_i . For domain i , we have

$$F\phi(\mathbf{r}') = \lim_{\delta \rightarrow 0} \int_{\Omega - \Omega_\delta} \frac{g(\mathbf{r}, \mathbf{r}')}{\chi_i} \varsigma_i(\mathbf{r}) dV - \int_{\Gamma} [\phi(dg/dn_i) - g(d\phi/dn_i)] dS, \quad (3.8)$$

where F equals 0, $\frac{1}{2}$, or 1, if \mathbf{r}' lies in Ω_i , on Γ , or outside Ω_i , respectively. Now, we multiply the above equation by χ_i , and we add the equations resulting for $i = 1$ and $i = 2$. Hence,

$$\left. \begin{array}{l} \mathbf{r}' \in \Omega_1 \\ \mathbf{r}' \in \Gamma \\ \mathbf{r}' \in \Omega_2 \end{array} \right\} \begin{array}{l} \chi_1 \phi_1(\mathbf{r}') \\ \frac{\chi_1 + \chi_2}{2} \phi_s(\mathbf{r}') \\ \chi_2 \phi_2(\mathbf{r}') \end{array} \Bigg\} = \int_{\Omega_1 + \Omega_2} g(\mathbf{r}, \mathbf{r}') \varsigma(\mathbf{r}) dV \\ + (\chi_2 - \chi_1) \int_{\Gamma} [\phi_s(dg/dn_1)] d\Gamma \\ + \int_{\Gamma} g(\mathbf{r}, \mathbf{r}') [\chi_1 d\phi_1/dn_1 - \chi_2 d\phi_2/dn_2] d\Gamma.$$

In case of an electrostatic problem, the part between brackets in the last term above equals the surface charge density on the boundary Γ , as can be seen by comparison with (2.63). Thus, it can be expected that the part between brackets equals the value of ς , interpreted as a surface source density.

To see that this is true in general, we can take the generalised Poisson equation (3.7), and construct the volume-integral over a cylindrical pill-box around the interface, where the height of the cylinder is limited to 0. Then, using the divergence-theorem, and noting that only the surface integrals over the top and bottom of the pill-box are nonzero under this limit, we see that, after subsequently limiting the radius of the pill-box to 0, that indeed, this reasoning is valid (or put differently, that we can derive this fact from the generalised Poisson's equation alone).

In the sequel, we will denote the surface source density as $\varsigma_{\text{surface}}$. Therefore,

we write the above as

$$\left. \begin{array}{l} \mathbf{r}' \in \Omega_1 \\ \mathbf{r}' \in \Gamma \\ \mathbf{r}' \in \Omega_2 \end{array} \right\} \begin{array}{l} \chi_1 \phi_1(\mathbf{r}') \\ \frac{\chi_1 + \chi_2}{2} \phi_s(\mathbf{r}') \\ \chi_2 \phi_2(\mathbf{r}') \end{array} \Bigg\} = \int_{\Omega_1 + \Omega_2} g(\mathbf{r}, \mathbf{r}') \zeta(\mathbf{r}) dV \\ + \int_{\Gamma} g(\mathbf{r}, \mathbf{r}') \zeta_{\text{surface}}(\mathbf{r}) d\Gamma \\ + (\chi_2 - \chi_1) \int_{\Gamma} [\phi_s(dg/dn_1)] d\Gamma \quad (3.9)$$

Although the above equation holds for a complex of only two materials, it can be easily extended to multiple materials. In general, for the potential ϕ in the interior of region i , we have

$$\begin{aligned} \bar{\chi}(\mathbf{r}') \phi(\mathbf{r}') &= \int_{\Omega} g(\mathbf{r}, \mathbf{r}') \zeta(\mathbf{r}) dV \\ &+ \int_{\Gamma} (\chi^+ - \chi^-) [\phi(dg/dn)] d\Gamma \end{aligned} \quad (3.10)$$

where the normal on Γ is chosen such that it points towards the material with constant χ^+ , and $\bar{\chi}(\mathbf{r}')$ is defined such that

$$\bar{\chi}(\mathbf{r}') = \begin{cases} \chi_i & (\mathbf{r}' \in \text{Int } \Omega_i) \\ \frac{\chi_i + \chi_j}{2} & (\mathbf{r}' \in \Gamma_{ij}). \end{cases} \quad (3.11)$$

Here, Γ_{ij} is the interface between domains i and j , and we assume for simplicity that no point lies in more than two different domain-boundaries at once (this poses no difficulties, as we will only be concerned with average potentials on surfaces and subvolumes). We stress that in (3.10), Ω is the complete domain including the interfaces. This allows us to incorporate the integral over the interfaces into the volume integral.

Also note that if we let the material parameter be invariant over the domain, then the surface integral in (3.10) vanishes, and we are left with our original formulation, (2.77), which was to be expected.

3.2.4 Method of Moments

The integral relation between ϕ and ζ of the previous section can be written using operator-notation, as

$$A\zeta = B\phi, \quad (3.12)$$

thus we have that

$$A\zeta \equiv \int_{\Omega} g(\mathbf{r}, \mathbf{r}') \zeta(\mathbf{r}) dV \quad (3.13)$$

$$B\phi \equiv \bar{\chi}(\mathbf{r}') \phi(\mathbf{r}') - \int_{\Gamma} (\chi^+ - \chi^-) [\phi(dg/dn)] d\Gamma \quad (3.14)$$

In case of a homogeneous domain with $\chi = 1$, we see that B degenerates to the identity operator, and comparing, in this case (3.12) to (2.75), we see that A is, in a sense, the “inverse” of the differential operator \mathcal{L} .

If we can discretize an operator-equation of the form

$$Ax = y, \tag{3.15}$$

then we can also discretize an equation of the form (3.12), since we can first treat

$$B\phi = y \tag{3.16}$$

in a similar fashion. Therefore, in the following, we assume that our basic equation is of the form (3.15), with $A : H_x \mapsto H_y$. First, we set up an orthonormal basis $\{x_n\}$ for the space H_x , and similarly, we define $\{y_n\}$ for the space H_y . Thus, we write

$$x = \sum_{n=1}^{\infty} \langle x, x_n \rangle x_n, \tag{3.17}$$

$$y = \sum_{n=1}^{\infty} \langle y, y_n \rangle y_n. \tag{3.18}$$

For the approximate solutions \hat{x} and \hat{y} , we write

$$\hat{x} = \sum_{n=1}^N \alpha_n x_n, \tag{3.19}$$

$$\hat{y} = \sum_{n=1}^N \langle y, y_n \rangle y_n, \tag{3.20}$$

where the coefficients α_n are to be determined. The approximation \hat{x} introduces an error e , so that $\hat{x} = x + e$. Thus, (3.15) can be written as

$$-Ae + \sum_{n=1}^N \alpha_n Ax_n = \sum_{n=1}^{\infty} \langle y, y_n \rangle y_n. \tag{3.21}$$

Note that since $Ax_n \in H_y$, we can write

$$Ax_n = \sum_{m=1}^{\infty} \langle Ax_n, y_m \rangle y_m. \tag{3.22}$$

Thus, we have

$$-Ae + \sum_{n=1}^N \alpha_n \sum_{m=1}^{\infty} \langle Ax_n, y_m \rangle y_m = \sum_{n=1}^{\infty} \langle y, y_n \rangle y_n. \tag{3.23}$$

Taking the inner product of both sides with y_k , we get

$$-\langle Ae, y_k \rangle + \sum_{n=1}^N \alpha_n \langle Ax_n, y_k \rangle = \langle y, y_k \rangle. \tag{3.24}$$

Now, if we choose α_n such that for all k

$$\sum_{n=1}^N \alpha_n \langle Ax_n, y_k \rangle = \langle y, y_k \rangle, \tag{3.25}$$

then obviously,

$$\langle Ae, y_k \rangle = 0. \quad (3.26)$$

Thus, by solving (3.25) for α_n , the residual Ae of equation (3.12) is implicitly orthogonalised to the test-functions y_k .

This does not necessarily mean that e becomes zero, of course, and not even that e converges to 0 if we let $N \rightarrow \infty$. However, for some important classes of operators, this convergence can be rigorously shown (see [7]).

3.2.5 Discretization

To apply the approach of the previous subsection, we will describe the computational domain using two-dimensional and three-dimensional elements. At the boundary of the domain, we will assume that two-dimensional panels are present. Accordingly, we partition the N elements into N_{surface} , N_{volume} , and $N_{\text{interface}}$, and the corresponding element numbers are contained in the sets $\mathcal{E}_{\text{surface}}$, $\mathcal{E}_{\text{volume}}$, $\mathcal{E}_{\text{interface}}$, respectively. Note that in a pure boundary-element approach, there are no volume elements, and then $\mathcal{E}_{\text{volume}} = \emptyset$. Further, we use \mathcal{V}_n to indicate the part of the domain occupied by element n (being either two or three-dimensional), and V_n to be its volumetric size.

For simplicity, the orthonormal basis-functions f_n will be chosen as

$$f_n(\mathbf{r}) = \begin{cases} 1/V_n & (\mathbf{r} \in \mathcal{V}_n), \\ 0 & (\text{otherwise}) \end{cases} \quad (3.27)$$

The volumes \mathcal{V}_n are chosen in an open sense, i.e., distinct volumes do not intersect (to keep the basis-functions orthonormal).

Further, we will use the Galerkin's approach, i.e., the test-functions are chosen equal to the basis-functions. Thus we have $\varsigma_n = \phi_n = f_n$, and we will use this to discretize (3.12). First, we will replace ς and ϕ in these equations by their approximate versions $\hat{\varsigma}$ and $\hat{\phi}$, which are defined by

$$\hat{\varsigma}(\mathbf{r}) = \sum_{n=1}^N \varsigma[n] f_n(\mathbf{r}), \quad (3.28)$$

$$\hat{\phi}(\mathbf{r}) = \sum_{n=1}^N (\phi[n] V_n) f_n(\mathbf{r}). \quad (3.29)$$

Note that in the latter equation, we incorporate a factor V_n to give $\phi[n]$ the meaning of a potential. Note that $\varsigma[n]$ already has the proper meaning (i.e., source-density times volumetric size). Thus for example, in the electrostatic case, ς may be a space charge density (units: $[C/m^3]$), and then $\varsigma[n]$ will be the total amount of charge in element n (units: $[C]$).

With these definitions in place, we can write (3.13) and (3.14) as, respectively,

$$A\varsigma(\mathbf{r}') \approx \sum_{n=1}^N \frac{\varsigma[n]}{V_n} \int_{\mathcal{V}_n} g(\mathbf{r}, \mathbf{r}') dV \quad (3.30)$$

$$B\phi(\mathbf{r}') \approx \sum_{n=1}^N \bar{\chi}(\mathbf{r}') \phi[n] V_n f_n(\mathbf{r}') - \sum_{n \in \mathcal{E}_{\text{interface}}} \phi[n] (\chi^+ - \chi^-) \int_{\Gamma_n} (dg/dn) d\Gamma \quad (3.31)$$

Note that the first integral over \mathcal{V}_n may be either a surface or a volume integral, depending on n . Equating both expressions, as in (3.12), and taking the inner product of both sides with the weighting function f_m , we obtain:

$$\begin{aligned} \chi_m \phi[m] &= \sum_{n=1}^N \frac{\varsigma[n]}{V_n V_m} \int_{\mathbf{r} \in \mathcal{V}_m} \int_{\mathbf{r}' \in \mathcal{V}_n} g(\mathbf{r}, \mathbf{r}') dr' dr \\ &+ \sum_{n \in \mathcal{E}_{\text{interface}}} \frac{\phi[n]}{V_m} (\chi_n^+ - \chi_n^-) \int_{\mathbf{r} \in \mathcal{V}_m} \int_{\mathbf{r}' \in \mathcal{V}_n} (dg/dn') dr' dr \end{aligned} \quad (3.32)$$

After dividing by χ_m , the above relation can be written in matrix-form, as

$$\mathbf{G}\boldsymbol{\varsigma} = (\mathbf{I} + \mathbf{H})\boldsymbol{\phi}, \quad (3.33)$$

where

$$g[m, n] = \frac{1}{\chi_m V_n V_m} \int_{\mathbf{r} \in \mathcal{V}_m} \int_{\mathbf{r}' \in \mathcal{V}_n} g(\mathbf{r}, \mathbf{r}') dr' dr, \quad (3.34)$$

$$h[m, n] = \begin{cases} \frac{(\chi_n^+ - \chi_n^-)}{\chi_m V_m} \int_{\mathbf{r} \in \mathcal{V}_m} \int_{\mathbf{r}' \in \mathcal{V}_n} (dg/dn') dr' dr & (m \in \mathcal{E}_{\text{interface}}), \\ 0 & (\text{otherwise}). \end{cases} \quad (3.35)$$

Note that, even though \mathcal{V}_i may have different dimensionalities, depending on i , the entries of \mathbf{G} have fixed units, due to the scaling factors. Similarly, the entries of \mathbf{H} have no units.

For simplicity, we will write the above equation as

$$\boldsymbol{\phi} = \hat{\mathbf{G}}\boldsymbol{\varsigma}, \quad (3.36)$$

and denote by $\hat{\mathbf{G}}$ the interaction-matrix

$$\hat{\mathbf{G}} \equiv (\mathbf{I} + \mathbf{H})^{-1} \mathbf{G}. \quad (3.37)$$

The integrand in (3.34) is the free-space Green's function, and thus it contains a singularity at $\mathbf{r} = \mathbf{r}'$. Fortunately, the integral exists. Several techniques are available to circumvent the singularity in the integral. An analytical technique to evaluate the inner integral over surfaces is described in [25]. Since the inner integral is finite, the outer integral can be performed using a quadrature scheme. See, e.g., [2].

The inner integral in (3.35) may be computed analytically simply by differentiating the analytical formula for the inner integral of (3.34). However, we recall that the integral has a discontinuity when \mathbf{r} crosses the surface \mathcal{V}_n , and this may complicate a practical numerical implementation of this integral. The main culprit here is that coordinates taken too closely to the surface may, due to numerical rounding, actually lie on either side of the surface, and thus may introduce a more or less random jump in the outcome of an evaluation performed during numerical integration. A solid implementation should take this effect into consideration.

Techniques for evaluating the integral in (3.34) in case g is the Helmholtz Green's function are described in [23], and they are improved in [27].

3.2.6 Computation of Resistive Effects

In this subsection, we will briefly review the computation of the resistive (or conductive) effects. The first step is to isolate the mechanism of conduction from the other electromagnetic effects. This implies that the Electro-Conductive (EC) regime, described in Section 2.8, is considered to be at work. Thus, we can use the generalised Poisson equation (2.35). Comparing this equation to (3.7), we see that the substitutions

$$\begin{aligned}\chi &\rightarrow \sigma, \text{ and} \\ \varsigma &\rightarrow I_{\text{in}}\end{aligned}$$

need to be made. To compute the resistive effects in a homogeneous, conducting metal-line with conductivity σ_{metal} , we discretize its boundary into panels. Each panel will have a normal pointing outward, and assuming that the surrounding material is perfectly insulating, we have that $\chi^+ = 0$ and $\chi^- = \sigma_{\text{metal}}$. Now we can apply (3.33). In this case, each element of the vector ς represents the total current into the corresponding panel, and each element of the vector ϕ represents the (average) electrostatic potential at the corresponding panel. Thus, essentially, the matrix

$$\mathbf{Y} \equiv \hat{\mathbf{G}}^{-1} \quad (3.38)$$

can be interpreted as an admittance matrix. Writing $\phi \rightarrow \mathbf{v}$ for the vector of voltages, and $\varsigma \mathbf{i}$ for the vector of currents, we have the familiar relation

$$\mathbf{Y}\mathbf{v} = \mathbf{i} \quad (3.39)$$

A corresponding circuit-model can be extracted more or less directly from the admittance matrix. However, we should remember that ϕ is a vector of absolute potentials, and not a vector of potential differences. After transformation, the circuit-model will consist of a set of resistors. Each resistor will have a positive value if the discretization is sufficiently fine. This follows from the diagonal-dominance property of the matrix \mathbf{Y} , as will be shown later.

Note that since we used a boundary-element approach, we obtain a resistor between every pair of panels on the boundary of the conductor. Thus, the amount of resistors could become excessively large for complicated interconnect-structures.

There are two ways to reduce the number of resistors. First, we can eliminate the nodes corresponding to panels on the boundary in which we are not interested (this will in fact electrically isolate these parts of the conductor).

Secondly, we can split the conductor into multiple subconductors, compute a model for them separately, and then join these models by electrically connecting the nodes corresponding to the interface-panels. If a conductor is split perpendicularly to the direction of the current, then only a single panel is required on the interface, since the electric potential can be considered constant across this interface. For very complex structures, the equipotential areas can be complex as well, and they can even vary depending on the stimuli. Nevertheless, for realistic conductors (with a long, stretched shape), we can simply take any cross-section of the conductor as a good approximation of an equipotential area.

Finally, we mention that a commonly used method to reduce the complexity of the circuit-model is to simply ignore small conductances (i.e., large resistors). A useful strategy is to ignore resistors between any pair of panels which are geometrically far apart (further than some threshold distance). Such resistors have small conductances, in general. Nevertheless, one should be aware that applying this strategy will inevitably introduce approximation errors, and this puts a strong bound on the threshold distance. In the case of long conductors, it is more effective to split the conductor into multiple parts, as described above.

Since on-chip interconnect has (generally) a very regular structure, we can of course split each conductor into smaller parts, precompute the circuit-models for a set of standard blocks, and store the resulting macromodels in a library. This is a known technique, and is discussed, for example, in [5] for the case of capacitance extraction.

3.2.7 Computation of Capacitive Effects

Here, we will briefly review the computation of capacitive effects. Again, we will isolate this electromagnetic mechanism from the other effects. The Electro-Static (ES) regime is at work in this case. See also Section 2.6.

As in the determination of the resistive effects, we will start with a generalized Poisson equation, in this case (2.31). Comparing this equation to (3.7), we see that the substitutions

$$\begin{aligned}\chi &\rightarrow \epsilon, \text{ and} \\ \varsigma &\rightarrow \rho\end{aligned}$$

are in order. Now, to compute the mutual capacitive coupling between a set of conductors, we partition their boundaries using panels, as before. Let us assume that the conductors are embedded in a single homogeneous dielectric with permittivity $\epsilon_{\text{dielectric}}$. Also assume that the panel-normals are pointing into the dielectric. Then, we can apply (3.33) with $\chi^+ = \epsilon_{\text{dielectric}}$, and $\chi^- = \epsilon_0$.

Note that often, for simplicity, the interior of the conductor is modelled to have the same permittivity as the surrounding dielectric¹. This is an approximation which is valid only when the resistivity of the conductor is reasonably low, since in that case capacitive self-couplings through the interior of the conductor become negligible.

In (3.33), the entries of the vector ς represent the total charge on each panel, whereas the entries of ϕ again represent the electrostatic potential at each panel. Thus, the matrix

$$\mathbf{C} \equiv \hat{\mathbf{G}}^{-1} \tag{3.40}$$

can be interpreted as a capacitance-matrix. Using the substitutions $\phi \rightarrow v$ (voltage), and $\varsigma \rightarrow \int i dt$ (charge), Equation (3.33) can be written in more familiar terms,

$$s\mathbf{C}\mathbf{v} = \mathbf{i}. \tag{3.41}$$

¹This is usually the case when the stratified dielectrics of an IC are modelled inside the Green's function, as in [18].

From \mathbf{C} , we can construct a circuit model comprised of capacitors. When the discretization is sufficiently fine, each capacitor is guaranteed to have a positive value, which is based on the diagonal dominance of the matrix \mathbf{C} .

Often, we are interested in the capacitance between two conductors, as opposed to the capacitance between separate panels on these conductors. Therefore, the elements in ϕ are usually partitioned according to the conductor to which their panels belong. Then, each set of potentials is mathematically forced to be equal, thus allowing the elimination of many entries in the matrix \mathbf{C} .

3.2.8 Computation of Inductive Effects

An important difficulty in computing inductive effects on a VLSI chip is that inductance is a property which is defined between closed current loops. However, it is hard, in practise to determine the exact paths of the current a priori (before simulation), and the task becomes even more difficult when we consider, e.g., ground planes, in which the current may take a different path, depending on the stimuli. Furthermore, since we will, as part of our method, decompose the VLSI chip into several smaller domains, current loops can become “cut” at the boundary of the domain.

Therefore, to compute the inductive effects, we will use the concept of partial inductances [16, 15]. This means, effectively, that we model the current in the system by discretizing the conducting material into filaments, i.e., regions in which the current is considered to flow in one direction only (or exactly the opposite direction), and furthermore, we will assume that the current is uniform per filament. Each volume of current induces a vector potential which is oriented in the same direction as the current, and the system is governed, in the Non-Retarded regime, by the vectorial Poisson equation (2.81). Thus, interactions are essentially between filaments only.

As explained, Equation (2.81) is actually composed of three scalar Poisson equations. In order to elegantly handle the vectorial nature of this equation, we write (3.33) into the form

$$\mathbf{G}\hat{\mathbf{i}} = (\mathbf{I} + \mathbf{H})\hat{\mathbf{a}}, \quad (3.42)$$

where $\hat{\mathbf{a}}$ is of dimensions $N \times 3$, and each of its rows represents the x , y , and z components of the (averaged) magnetic vector-potential in the corresponding filament. The matrix $\hat{\mathbf{i}}$ is also of dimensions $N \times 3$, and each of its rows is of the form

$$\hat{\mathbf{i}}[m, *] = I_m l_m \mathbf{x}_m^T. \quad (3.43)$$

Here, I_m is the current through filament m , l_m is the physical length of filament m , and \mathbf{x}_m is a normalised vector pointing into the direction of the current of filament m . Note that we assume in the case of inductive effects that filaments have a rectangular shape, or a cuboid shape if they extend in three dimensions, and thus l_m is well-defined.

In order to relate the magnetic vector potentials to the induced voltages in each filament, we use (A.9), where we note that the magnetic contribution to the electric field comes from the term $s\mathbf{A}$. Integrating this term along the length of filament m gives us the induced voltage in the filament,

$$v[m] = s \int \mathbf{A}_m \cdot d\mathbf{l}_m, \quad (3.44)$$

or

$$v[m] = sl_m \hat{i}[m, *] \cdot \mathbf{x}_m^T. \quad (3.45)$$

Then, by some algebraic manipulation, and using the above equations, we can write (3.42) as

$$\mathbf{v}_{\text{branch}} = s\mathbf{L}\mathbf{i}, \quad (3.46)$$

where $\mathbf{v}_{\text{branch}}$ is the $N \times 1$ vector of filament potential-differences, and \mathbf{i} is the $N \times 1$ vector of filament currents, and

$$l[i, j] = \hat{g}[i, j] l_i l_j (\mathbf{x}_i^T \cdot \mathbf{x}_j), \quad (3.47)$$

using the definition (3.37). The matrix \mathbf{L} is called the partial inductance matrix, and each of its diagonal elements $l[i, i]$ represents the self-inductance of the corresponding filament i , while its off-diagonal elements $l[i, j]$ represent the mutual-inductance between filaments i and j . The matrix \mathbf{L} may be considered symmetric when the discretization is sufficiently fine, since then $\hat{\mathbf{G}}$ will be symmetric as well, and (3.47) is symmetric in i and j .

3.2.9 Passivity of the System

In the above, we have extensively used the generalized Poisson equation to model the electromagnetic effects. Since this lead to a simplification of the full-wave equations, it is interesting to see if we can find useful properties which hold for both the simplified and the original case. One of the useful properties is that of passivity, i.e., it is important that our resulting system does not produce energy, but merely consumes, or conserves energy.

If we assume a homogeneous domain, then (3.7) reduces to the regular Poisson equation

$$\Delta\phi = -\varsigma/\chi. \quad (3.48)$$

Now in the electrostatic case, the energy stored in a given charge-distribution is given by the volume integral

$$U_e = \frac{1}{2} \int_{\Omega} \phi(\mathbf{r}) \rho(\mathbf{r}) d\Omega, \quad (3.49)$$

whereas in the magnetic case, the energy stored in a distribution of currents is given by

$$U_m = \frac{1}{2} \int_{\Omega} \mathbf{A}(\mathbf{r}) \cdot \mathbf{J}(\mathbf{r}) d\Omega. \quad (3.50)$$

Thus, if we wish to show that these energies are nonnegative, then proving that

$$\int_{\Omega} \phi(\mathbf{r}) \varsigma(\mathbf{r}) d\Omega \geq 0 \quad (3.51)$$

is sufficient. Using Green's first Theorem (A.26) and setting $u \rightarrow \phi$, and $w \rightarrow \phi$, we have

$$\int_{\Omega} \phi \Delta\phi d\Omega = \int_{\partial\Omega} \phi(d\phi/dn) dS - \int_{\Omega} \nabla\phi \cdot \nabla\phi d\Omega. \quad (3.52)$$

For an infinite domain, the first term on the r.h.s. can be eliminated under proper conditions, thus on the boundary ϕ should converge to 0 sufficiently fast, which is possible to achieve. Further, we see that the integrand of the remaining volume-integral on the r.h.s. is of a quadratic form, and hence the integral is nonnegative. Finally, using (3.48) on the l.h.s., we see that (3.51) is true. Hence also,

$$U_e \geq 0 \text{ and } U_m \geq 0. \quad (3.53)$$

In discrete form, Inequality (3.51) can be expressed as

$$\phi^T \cdot \varsigma \geq 0. \quad (3.54)$$

Of course, this expression may not hold when discretization errors occur, but we will assume that the discretization is so fine that it is true (at least for engineering purposes). Using (3.36), we have that

$$\phi^T \hat{\mathbf{G}}^{-1} \phi \geq 0. \quad (3.55)$$

Since we are free to choose ϕ , the above equation makes explicit that the interaction-matrix $\hat{\mathbf{G}}^{-1}$ is positive semi-definite. Since $\hat{\mathbf{G}}^{-1}$ is invertible, this matrix is actually positive definite. The conductance matrix \mathbf{Y} (3.38) and the capacitance matrix \mathbf{C} (3.40) share this property.

We cannot directly translate the positive definiteness property to the inductance matrix \mathbf{L} , since its derivation is different from that of the $\hat{\mathbf{G}}$ matrix. In fact, in (3.47), we see that each entry of $\hat{\mathbf{G}}$ is essentially multiplied by a scalar-product $\mathbf{x}_i^T \cdot \mathbf{x}_j$, and the two lengths of the filaments l_i and l_j , which complicates the analysis. However, we can rewrite (3.46) using (3.44), to obtain the relation

$$\begin{bmatrix} \int \mathbf{A}_1 \cdot d\mathbf{l}_1 \\ \vdots \\ \int \mathbf{A}_n \cdot d\mathbf{l}_n \end{bmatrix} = \begin{bmatrix} l[1,1] & l[1,2] & \dots \\ l[2,1] & l[2,2] & \dots \\ \vdots & \vdots & l[n,n] \end{bmatrix} \begin{bmatrix} i[1] \\ \vdots \\ i[n] \end{bmatrix} \quad (3.56)$$

Now, multiplying both sides of the above equation from the left by \mathbf{i}^T , and noting that \mathbf{i} is a discretized form of the current density \mathbf{J} , we see using (3.50) that

$$\mathbf{i}^T \mathbf{L} \mathbf{i} \geq 0. \quad (3.57)$$

Again, \mathbf{L} is invertible and since we can choose \mathbf{i} arbitrarily, \mathbf{L} is positive definite.

3.2.10 Diagonal Dominance

The matrix $\hat{\mathbf{G}}$ is positive definite as discussed in the previous section, but its inverse has another important property, namely that of diagonal dominance. This fact is well-known, however whether it carries over to the inductive case, and in particular the case of arbitrarily oriented current-filaments, is not so clear.

Let us first consider the capacitive case. The value of the diagonal entry $c[i, i]$ of the capacitance matrix can be determined by setting the potential of panel i to unity and the potential at the other panels to zero. Then the amount of charge at panel i will be numerically equal to $c[i, i]$. A special property of the Laplace equation is that, for an arbitrary volume V containing no sources, the maximum and minimum

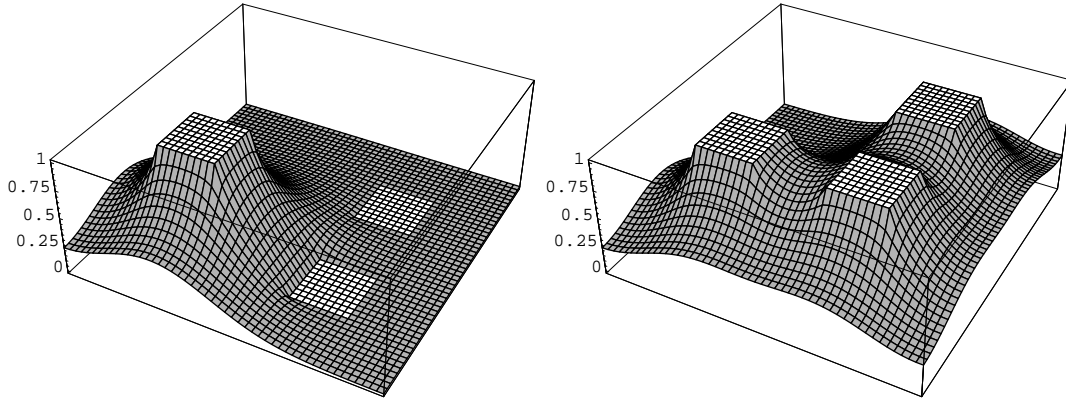


Figure 3.1: Solution to the Laplace equation in two-dimensions, where (a) one panel is set to unit potential, and (b) all panels are set to unit potential.

potential is found on the boundary ∂V . This means that panel i , being the only panel at unit potential, will have a potential which is a global maximum over the domain. See also Figure 3.1. Thus, on the panel boundary,

$$\frac{\partial \phi}{\partial n} < 0. \quad (3.58)$$

We will use this fact by integrating the Poisson equation (3.48) around the panel,

$$\int_P \nabla \cdot \nabla \phi dV = - \int_P \varsigma / \chi dV, \quad (3.59)$$

and then applying Gauss' law to the r.h.s., to obtain

$$\int_{\partial P} \nabla \phi \cdot d\mathbf{S} = -\frac{1}{\chi} \int_P \varsigma dV. \quad (3.60)$$

The r.h.s. is strictly negative because of (3.58). The integral on the l.h.s. represents the charge on the panel, and thus this charge must be positive (χ , in this case the permittivity, is positive). This means, in turn that the diagonal entries $c[i, i]$ are positive.

Using a similar argument, we can see that the off-diagonal entries are negative: when setting a panel to unit potential and the other panels to zero potential, then the charge on the other panels must be negative. Finally, the sum of entries in each row of C must be nonnegative, which we can see by setting all panels to unit potential, and noting that the potential at infinity is zero.

Of course, these arguments hold not only for the capacitive case, but for any instance of the Poisson equation, (3.48). Also note that a diagonal dominant matrix with positive entries on its diagonal is positive definite (but the reverse is not generally true). This is in accordance with the previous subsection.

For the inductive case, the matrix \hat{G} is applied differently, i.e. (3.47) is not used directly in the constitutive equations (3.46). To get the equivalent of the capacitance matrix, we will write the system as

$$\begin{bmatrix} k[1, 1] & k[1, 2] & \dots \\ k[2, 1] & k[2, 2] & \dots \\ \vdots & \vdots & k[n, n] \end{bmatrix} \begin{bmatrix} \int \mathbf{A}_1 \cdot d\mathbf{l}_1 \\ \vdots \\ \int \mathbf{A}_n \cdot d\mathbf{l}_n \end{bmatrix} = \begin{bmatrix} i[1] \\ \vdots \\ i[n] \end{bmatrix}, \quad (3.61)$$

so that

$$\mathbf{K} = \mathbf{L}^{-1}. \quad (3.62)$$

is the inductive equivalent of the capacitance matrix.

In this case, off-diagonal entries may be positive, since setting for example the electric branch-potential $v[2]$ to 1, and the other potentials to zero, means that the vector potential at panel 2 is directed in the same general direction as the orientation vector \mathbf{x}_2 of this panel. This does not mean that the x, y, z components of \mathbf{A}_2 are positive.

The conclusion is that if panels are arbitrarily oriented, we cannot make a statement about the diagonal dominance of the \mathbf{K} matrix. In fact, it has been shown by experiments that \mathbf{K} is actually *not* diagonally dominant in general. However, we can still see that the diagonal entries of \mathbf{K} are positive, by using a similar argument as for the electrostatic case (or we can see it from the fact that \mathbf{K} is positive-definite).

Since \mathbf{K} is not diagonally dominant, it is not possible to truncate off-diagonal entries in this matrix without risking that it loses the positive definite property. This will be an important issue.

A simple trick exists to make \mathbf{K} diagonal dominant: simply align the filaments along three orthogonal axes. Then, the inproduct of the direction-vectors of two filaments will be either 1 or 0, and \mathbf{K} (as well as \mathbf{L}) will consist of a 3×3 diagonal block-matrix. See for example [1], [26]. Although, in principle, any layout can be decomposed into an orthogonal set of filaments, such a technique can only be applied reasonably well for designs which have intrinsically orthogonal geometries.

3.2.11 Boundary Element Acceleration Techniques

When computing an equivalent circuit-model, we first need to compute the Green's matrix \mathbf{G} as explained. This computation takes $\mathcal{O}(N^2)$, where N is the number of elements in our domain. The next step is the inversion of the Green's matrix, which takes even more effort, i.e., this operation is of order $\mathcal{O}(N^3)$. This large effort may be compensated by the reduction of N using domain-decomposition (this will be discussed in the next chapter). If N can be bound below some constant, then the computational effort can be reduced to $\mathcal{O}(1)$ per subdomain, in theory.

Other techniques have been proposed to reduce the computational effort of the boundary-element method. Popular techniques are the Fast Multipole Method (FMM) and the precorrected FFT (pFFT) method [14], which will be outlined shortly.

Consider the constitutive equation for capacitance, (3.39). First, we avoid explicit computation of $\mathbf{C} = \hat{\mathbf{G}}^{-1}$ (3.38) and hence we state the equation in the form

$$(1/s)\hat{\mathbf{G}}\mathbf{i} = \mathbf{v}, \quad (3.63)$$

and to aid the discussion, we simplify the equation to

$$\hat{\mathbf{G}}\mathbf{q} = \mathbf{v}, \quad (3.64)$$

with $\mathbf{q} = (1/s)\mathbf{i}$ the vector of charges.

Iterative approaches for solving an equation of the form $\mathbf{Ax} = \mathbf{b}$ have as primary cost per iteration the multiplication of \mathbf{A} by a vector. Normally such a multiplication costs $\mathcal{O}(N^2)$, where N is the number of panels. Using FMM, the product can be performed in $\mathcal{O}(N)$ instead.

In principle, a multiplication $\hat{\mathbf{G}}\mathbf{x}$ can be interpreted as the computation of the potential at every panel, given a charge-distribution \mathbf{x} . The effect of the charge-distribution is computed by superposition, i.e., for a given panel i , we compute the potential by summing the effects of the charges. The acceleration technique used by the FMM is to group charges (panels) which are at a certain distance from the test-panel i , and instead of summing the effects of the charges to the potential at i individually, we determine the effect of the group of charges at once, by using multipole-expansions. For distant groups, this computation can be done with the same accuracy but with less effort than taking the individual charges into account. By performing the grouping in a clever way, the FMM can attain a linear computational complexity for the matrix-vector multiplication (even if the panels are distributed over the domain in an inhomogeneous fashion).

The pFFT method works in a similar way. Again panels are grouped, but instead of using the multipole-expansions to model the effect of a group of charges, we project the charges onto the vertices of a grid. That is, the effect of the charges in a group are modelled by a set of charges at fixed locations. Then, the effect of the grid-charges on the potential at all other grid-points is computed by performing a convolution-operation. This convolution is efficiently performed in the Fourier-transformed domain by applying a Fast Fourier Transform twice. Finally, the potentials at the test-panels are computed by interpolating the potentials at the grid-points.

Of interest is that White et al. [24] have made a comparison between the FMM and pFFT methods. Their conclusion is that pFFT is faster for small problems, but since it has an expected $\mathcal{O}(N \log N)$ time complexity, compared to $\mathcal{O}(N)$ worst-case for the FMM, it will be outperformed for larger N . The break-even point, however, is expected not to be reached for most engineering problems.

Of course, the acceleration techniques mentioned can be used for other problems than capacitance extraction. If the kernel used in the integral-formulation is of the form $1/r$ or of the form $(\partial/\partial n)(1/r)$, then in principle the techniques can be applied. It is trivial to convert the problem from a capacitive problem to a conductive problem, since (3.40) and (3.38) are structurally similar. Inductive problems can be treated largely in an analogously fashion, but due to the vectorial nature of the fundamental equation (2.81), some additional tricks are necessary [9].

In our situation, where we have a lot of small domains for which we first need to compute compact models and consequently need to merge those domains, these integral acceleration techniques are not completely appropriate. The reason is that for small domains, it is not worthwhile to group “distant” charges, since only small distances exist. However, what exactly is to be considered “small” remains to be investigated, so the techniques may be of practical use. Nevertheless, it is clear that these techniques will have no dramatic impact on the asymptotic computational complexity of our method.

Besides the above techniques, it is sometimes possible to exploit the structure of the domain, and reduce thereby the number of required panels. One way

in which this can be done, is by incorporating information about the domain in the Green's function. For example, [18] describes a technique that solves the capacitive and substrate-resistance problems using domain-specific Green's functions. For the substrate problem, this means that no interface panels are needed in the interior of the substrate in order to model the doping profile. The savings in terms of the dimensions of the resulting matrix can be considerable, but depend ultimately on the complexity of the substrate profile. On the other hand, generally it takes considerably more effort to evaluate the domain-specific Green's functions than to evaluate the free-space Green's function.

Another structure-exploiting technique has been described in [4]. This paper discusses the substrate-resistance extraction problem. Similarly as above, the treatment of the doping profile is incorporated into a domain-specific Green's function. Then, the top of the substrate is divided into a grid of rectangular panels, and the Green's function matrix is built for these panels. It turns out that the continuous equivalent of this matrix has eigenfunctions which coincide with the expansion-functions in a two-dimensional discrete cosine transform (DCT). The main result is that the multiplication by the Green's matrix can be accelerated by performing a DCT and an inverse DCT. These operations have $\mathcal{O}(N \log N)$ complexity, and thus are much faster than direct multiplication. The drawback of this technique is that it applies only to a substrate which is discretized into a grid of rectangles. This means that in practise, the number of panels may become excessively large.

3.3 Finite Difference/Integrals Methods: FDM/FIT

The previous section discussed the boundary-element method, which is essentially a surface-based technique. We will now focus on a volume-based technique, namely the Finite Difference Method/Finite Integration Technique (FDM/FIT).

The Finite Difference Method usually involves approximating the differential equations by difference equations on a rectangular grid. However most papers start from the global forms of Gauss, Ampere or Faraday laws, using actually the simpler and most robust Finite Volume Methods or Finite Integrals Technique to derive their linear system of equations.

The deliverable [D1.2] presented in detail how this method is applied in the modelling of the integrated passive components. This is why the present paragraph is focused mainly on the modelling of a particular environmental component, the substrate. Metallic interconnects will be analyzed together with their EM coupling with the substrate.

Applied in the static regimes this category of methods generates an equivalent circuit having 6 branches for each grid-node. Figure 3.2 depicts this circuit for the case of EC regime. The method may be applied also in EQS regime (Fig. 3.3) and even in FW regime (Fig. 3.4).

The EQS model results in a 3D mesh where each edge is a parallel combination of a resistor and a capacitor, as shown in Fig. 3.3 and Fig. 3.4.a. The full-wave model results, according to [21], in a distributed RLC equivalent circuit, as shown in Figure 3.4, where "voltage" corresponds to the magnetic potential A . We note that parameters RLC do not correspond to physical resistors, inductors, capacitors and

are measured in units of Siemens/ m^2 , Farad/ m^2 , and Henry $\times m^2$ respectively. The lumped circuits are fed with current-controlled voltage sources with trans-resistance Z_{ij} . The resulting coupled circuit equations are solved with one of the standard methods. A different purely resistive magnetic vector-potential equivalent circuit has been proposed by Pacelli in 2002 for the modelling of inductive parasitics between wires. A similar approach to represent the discrete form of the Maxwell equations as a pair of coupled circuits, one electric and other magnetic is proposed in [10].

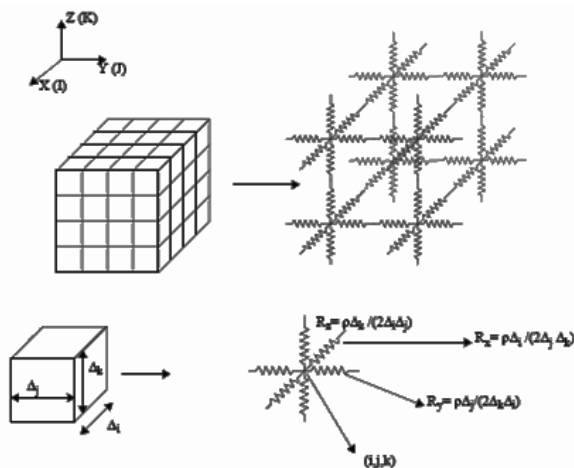


Figure 3.2: Equivalent network of the substrate in EC regime [6]

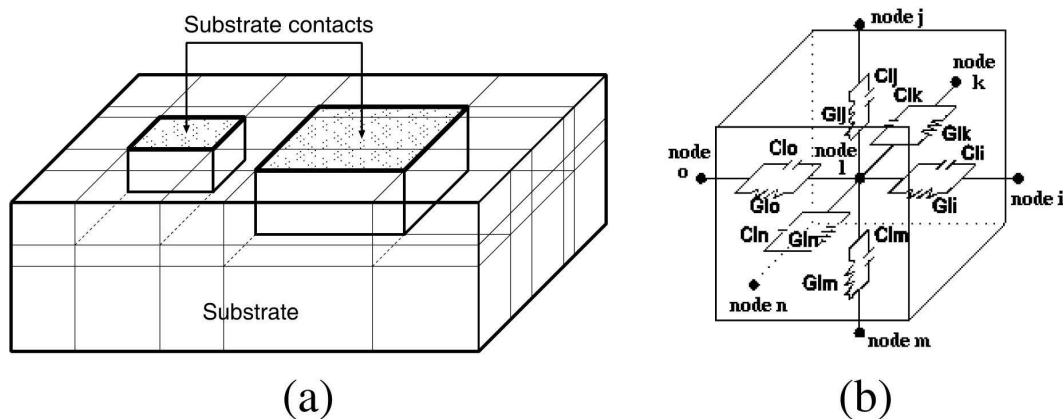


Figure 3.3: Equivalent RC network of the substrate in EQS regime [17]

Determining a suitable rectangular grid for the substrate is a difficult problem. If the number of the surface contacts is large or the dimensions of the contacts are small, then using a uniform grid may not be practical. For example, if the minimum contact size is $5\mu m$ on a $1000 \times 1000 \times 500\mu m^3$ substrate, the number of grid points, assuming a uniform grid, will be at least $n = 200 \times 200 \times 100$ that is four million. This can lead to prohibitive matrix sizes. A common strategy to deal with this problem is to make the grid dense in the areas where the variation in the potential is expected to be large and make the grid coarse where the potential variation is small. For example, the grid may be made dense around sharp corners, or in the vicinity of contacts, and coarse in regions away from the contacts. This scheme helps reduce the size of the matrices involved. The problem with the technique is that it is difficult to determine beforehand the regions where the field is high. Another approach is to

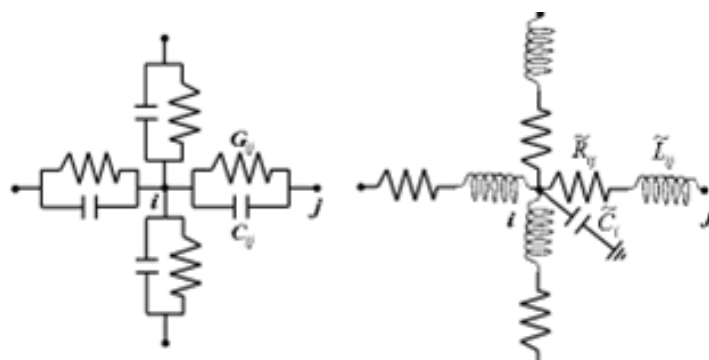


Figure 3.4: Equivalent electric and magnetic networks of the substrate in FW regime (only four of six nodes connected to the central node are shown) [21]

use progressively denser grids until the error is tolerable. This may not always be a good solution since it may require considerable computation too.

An alternative is considered the Finite Element Method (FEM), where the discretization mesh has as basic element triangle or tetrahedral. It is more flexible than the rectangular mesh [12], [13].

The next step in the process is the *solution of the linear system of equations*. This is the most computationally intensive step in the problem. Several direct and iterative techniques are used to solve sparse linear systems of equations.

Direct techniques for solving a linear system of equations include Gaussian elimination and LU factorisation. These techniques are unsuitable for solving the substrate problem because their computational complexity is $O(n^3)$ for dense systems, where n is the number of total nodes in the grid. Although substrate conductance matrices are sparse, the matrices can be of a very large order and the solution techniques used must be able to exploit sparsity in order to avoid excessive demands on the computer storage. By using the sparse techniques the order of the solving time decreases to $O(n^2)$.

Iterative techniques used in the solution of sparse matrices have been discussed extensively in the past. Iterative techniques have the advantage that they work with the system matrix, without modifying the matrix significantly. If the matrix is sparse to begin with, the sparsity is preserved throughout the solution procedure. Iterative techniques generally start with an initial approximation to the solution vector. The technique converges towards the solution vector, through a sequence of iterative steps. The convergence is asymptotic and an infinite number of iterations are required to converge to the solution vector. In practise, however, a fairly good approximation to the correct solution can be achieved by truncating the iteration once a pre-decided error threshold is reached. *The Conjugate Gradient Algorithm is one of the most appropriate* iterative scheme for solving the large matrices which result from the finite differences technique. The objective to obtain a solving time of order $O(n)$ may be reached (Table 3.1). "However, despite all of the simplifying assumptions made earlier, the solution of substrate problems with more than ten-to-twenty contacts becomes impractical. Due to this reason the finite-differences technique was not used for substrate parasitic extraction" is a conclusion of [6]. Preconditioning is particularly important for large Laplace/Poisson type problems because the condition number of their discrete form grows quadratically with the discretization fineness.

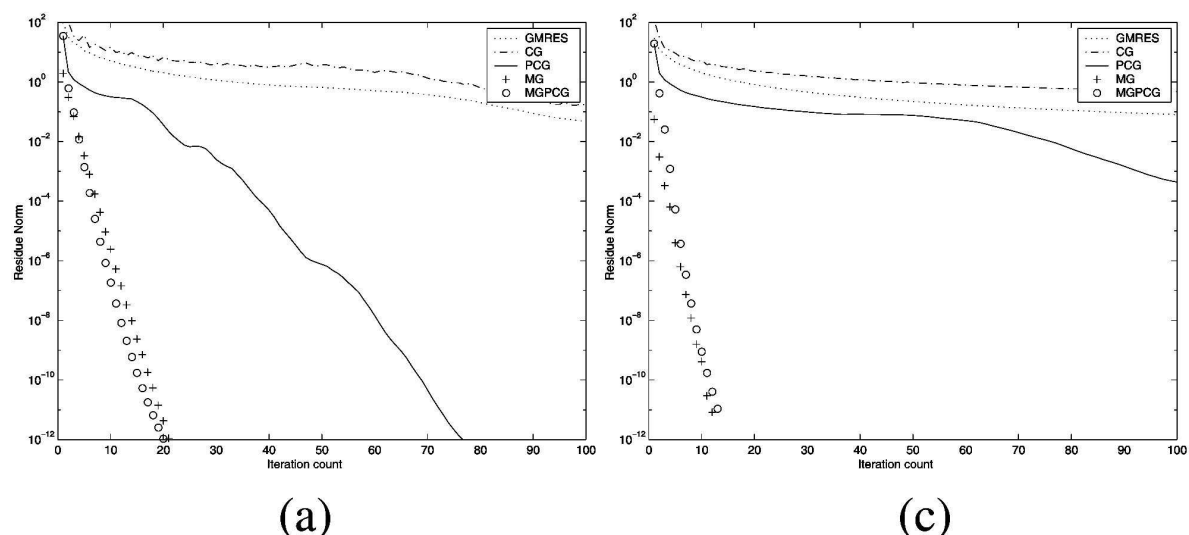
Technique	Memory	Computation time (s)	Resistance (Ω)
FD (3920 pts.)	19k	15	233
FD (6480 pts.)	32k	35	273
FD (13520 pts.)	67k	75	298
FD (35280 pts.)	176k	180	311
FD (109520 pts.)	547k	674	318
Green function	10k	190	345
DCT	263k	1	340

Table 3.1: Resistance of a single contact to the backplane using three techniques to solve the linear system of equations

Fast Poisson solvers are the methods of choice for solving problems with uniform boundary conditions in each dimension. Unfortunately they *cannot be applied* directly to problems, such as ours, with *irregular mixed boundary conditions*. However, for a preconditioner to be effective it only needs to be an *approximate inverse*, suggesting the use of a fast Poisson solver *for the pure-Dirichlet problem* as a preconditioner [11]. In that work are described numerical experiments for substrates with solutions having 10^{-5} relative residual tolerance obtained in about 20 iterations for substrates having 1000-4000 contacts. As concluded in [11], the proposed method is effective for substrate-model extraction because the system matrix is quite sparse (at most 7 nonzeros per row) and thus cheap to apply, and because it allows a good preconditioner.

In [17] *Multigrid (MG) methods* are used and their efficiency is compared to Krylov-subspace methods, such as Conjugate Gradient (CG). It is well known that the performance of Krylov-subspace methods can be further improved if a good preconditioner can be obtained. Incomplete Cholesky factorisation demonstrated to yield the efficient behaviour and was thus used as a preconditioner (PCG). Actually the Multigrid method itself can also be used a preconditioner (and we term that MGPCG).

MG methods are based on the different accuracy on several grids. Starting from a fine 3D mesh, the solution is successively projected to coarser grids until the grid became enough small to allow an efficient direct solution (e.g. by Gauss elimination). Solutions obtained for any coarser level are then interpolated to finer levels where local solutions are adjusted. This is called a MG V-Cycle. MG based methods converge in a constant number of iterations, while CG and PCG show rapidly degrading of the convergence order and of computational complexity, This is the main advantage of using Multilevel methods to solve the substrate coupling problem. As Krylov-subspace methods have $O(n)$ time complexity, this time saving ratio will quickly increase for finer and finer discretizations. The convergence speeds of several methods are compared in Fig. 3.5. The main drawback of using MG-based methods is their memory requirements. These methods need to keep not only projection and interpolation operators in memory but all levels matrices and vectors also. It can be shown that these structures memory requirements are limited to the double amount of the finer level structures memory. This leads to MG-based methods showing approximately double memory requirements of Krylov-subspace methods [17].



Method	33×33 ×17	65×65 ×33	129×129×65
CG	2.55	31.20	369.14
PCG	1.09	13.52	189.30
MG	2.65	18.55	140.20
MGPCG	2.26	17.09	136.08

Figure 3.5: Evolution of the residual norm and the table of the solving time [17]

3.4 Comparison of BEM and FDM/FIT

Advantages of BEM

- BEM is very appealing, since it effectively reduces a 3D problem to a 2D one, requiring only a surface discretization.
- It is possible to use, instead of the free-space Green's functions, specialised Green's functions for the modelling of inhomogeneous domains, where only part of the interfaces are discretized. For example, for a stratified approximation of a doped substrate, only the top surface may be discretized, and the material-interfaces below the surface may be treated using a domain-specific Green's function. See for example [18].
- Any specialised Green's functions may be precomputed, and tabulated for fast lookup during extraction.
- Certain interfaces need not be discretized if they are sufficiently far from the problem-domain. For example, in substrate extraction, often side-wall effects may be neglected.
- The linear system allows efficient pre conditioners for the iterative solution of the linear systems obtained by the BEM [20].
- Sparsification techniques can be applied to alleviate the multiplication of vectors by the dense Green's matrix, in iterative solution schemes. The FMM and pFFT methods may be used for example.

- For the case of substrate-extraction, where the contact-panels are essentially on a flat surface, the discretized Laplace operator can be decomposed in an eigenvalue-decomposition. Then, application of the matrix G to a vector of currents can be accelerated by applying the (inverse) 2D DCT. The result is an $O(N\log N)$ time complexity for the multiplication operation.
- Multigrid methods, or more generally, multilevel methods, are known to be the most efficient iterative techniques in the solution of the elliptic partial differential equations. They were adapted for first-kind integral-equations. The efficiency of multigrid methods is a direct consequence of the fact that the convergence rate is independent of the discretization, and hence the problem size. See also, e.g., [3].

Drawbacks of BEM

- The matrix of the linear system generated by the BEM is dense.
- When specialised Green's functions are used, for example to model the substrate doping-profile, the versatility in terms of allowed geometry is reduced. Complex conductivity structures, such as wells, diffusion gradients, and buried layers cannot be handled by using this technique.
- It is difficult to enforce hybrid Dirichlet/Neumann boundary conditions. Such conditions are useful for substrate modelling.
- Direct evaluation of specialised Green's functions is an expensive task. For multi-layer structures, and depending on the technique used, the evaluation may require a large amount of floating point operations, since these functions are usually a large expansion of complex terms.
- The modified Galerkin solution procedure utilised in the BEM could become ill-conditioned because the singularity of sources at panel-boundaries cannot be accommodated with uniformly-sized panels.
- The determination of the most suitable grid of panels is not an easy problem.
- The application of the 2D-DCT technique mentioned can only be applied for a uniform discretization of ports. This results in the discretization to be much finer than desired.
- Inversion of the Green's function matrix may be a cumbersome task, although acceleration techniques such as FMM and pFFT may be used to speed up iterative solution techniques.
- Krylov-subspace iterative methods converge slowly when applied to large BEM systems, which tend to be ill-conditioned.

Advantages of FDM/FIT

- Finite difference schemes are attractive for their simplicity of use and versatility in handling virtually any type of substrate profile.

- Modern process technologies produce substrates with complex conductivity profiles as a result of features such as wells, diffusion gradients, and buried layers, which can be discretized easily by FDM/FIT.
- FDM/FIT allows a natural representation of mixed Dirichlet-Neumann problems.
- The matrix of the linear system generated by FDM/FIT is quite sparse (at most 7 nonzeros per row) and thus cheap to apply.
- The linear system allows efficient preconditioners.
- This type of methods has also been recently enhanced with fast solution techniques.

Drawbacks of FDM/FIT

- Determining a suitable FDM/FIT grid for the substrate is a difficult problem.
- Although sophisticated discretization schemes (other than a simple rectangular one) can be used to eliminate the generation of mesh nodes in regions where they are unnecessary, such schemes come at added computational expense.
- Mesh sizes required for accurate extraction become too large too quickly, with increasing domain size.
- In FD or FEM methods, the whole 3D volume of the substrate is discretized leading to large matrices. Fortunately, contrarily to BEM methods, FD/FEM methods produce large yet sparse matrices which nonetheless require extensive memory resources.

4 Conclusions

In this deliverable, we have reviewed techniques which have been proved useful in the realization of Task 2.1 of the Chameleon-RF project.

First, we have described how the modelling-approach may be varied across the computational domain, such that the assumed model is (locally) of the lowest complexity, while it does not compromise the required accuracy. It is also reviewed how the obtained sets of partial differential equations are converted to a discrete form, solvable by a computer.

Within the framework set up in this deliverable, there is room for many computational optimizations, and many of these have been exploited in our project. Since the scope of this document is restricted, we did not describe them here. However, we can make some interesting remarks.

First, the domain-decomposition approach (described in detail in earlier deliverables) may be applied to reduce the computational complexity by identifying equi-potential surfaces. Such surfaces may be found in approximation by inspecting the local geometry of the problem. Here the potential can refer to any potential, not just the electric scalar potential, but also the magnetic vector-potential, or the magnetic scalar potential. On each equi-potential surface, only a small amount of variables (usually only one) is necessary to describe the potential, and thus such an approach can reduce the overall number of degrees of freedom. Adaptation of the discretization to the local geometry is an essential tool in physics-based model reduction.

Domain-decomposition is also an essential tool for reducing the computational complexity of the BEM. Since the BEM produces models of order $\mathcal{O}(N^2)$, where N is the number of boundary panels, we may split the domain into smaller parts, such that the complexity approaches $\mathcal{O}(N)$. Because domain-decomposition introduces new variables on the interfaces between domains, there obviously exists a trade-off, and it can be exploited. This approach stands in contrast with the traditional kernel-interpolation approaches such as the Fast Multipole Method, which require intervention in the linear solver (where the matrix-vector product is optimized).

As a further step, we may apply domain-decomposition to simplify and speed-up the model-extraction process. The computational domain is physically sliced into regular blocks, such that identical models can be emitted for equal blocks. In realistic vlsi designs, there is much geometrical repetition and therefore this technique may be quite advantageous.

For modeling the metallic interconnect, a highly efficient optimization is the reduction of the model to a two-dimensional one. Such an approximation is justified in many cases since the interconnect is usually composed of long sections in which the cross-section does not vary. Essentially, we can then obtain the parameters in an equivalent transmission-line model, and use these to obtain a discrete model for the interconnect. This model can of course also include coupling to the underlying substrate.

Although only briefly touched upon in this document, substrate effects are also essential in describing the coupling between on-chip components. For relatively low frequencies, up to several tens of GHz, we may use a BEM formulation, which

is common in the literature. For higher frequencies, the FIT method described in this document may be applied. Again, the exploitation of the geometrical structure is essential in obtaining an efficient model. Since the substrate is only excited at its top surface, the discretization can be exponentially reduced towards the bottom of the substrate, such that a model of approximately $O(N \log N)$ complexity is obtained, where N is the number of panels at the top surface.

A Miscellaneous Derivations and Formulae

This appendix contains various derivations and formulae which are used throughout the main document.

A.1 Space-charge Distribution

Here, it is explained using a standard argument that space-charge ρ is inherently located at material interfaces only (we assume that all material changes are abrupt). This confinement of charge is an important fact, since it allows us to conveniently rewrite volume integrals into surface integrals in cases where the space-charge density can be factored from the integration kernel.

The argument is as follows. Since we assumed μ to be constant, we are only interested in the surfaces where either the conductivity σ or the permittivity ϵ has a transition. Inserting (2.5) into (2.2) and taking the divergence on both sides, we obtain

$$j\omega\nabla \cdot \epsilon\mu\mathbf{E} + \nabla \cdot \mu\sigma\mathbf{E} = 0. \quad (\text{A.1})$$

At locations in the domain where there is no interface, we have that σ and ϵ are constant, and hence we may factor the above equation as

$$(\nabla \cdot \mathbf{E})(\sigma + j\omega\epsilon) = 0. \quad (\text{A.2})$$

At nonzero frequency or at nonzero σ , we find that

$$\nabla \cdot \mathbf{E} = 0. \quad (\text{A.3})$$

Now, from (2.7) and (2.4), and taking ϵ constant, we have that

$$\nabla \cdot \mathbf{E} = \frac{\rho}{\epsilon}. \quad (\text{A.4})$$

Comparing (A.3) and (A.4), we see that

$$\rho = 0 \quad (\text{A.5})$$

at locations where there is no transition in material parameters.

A.2 Potential-functions and Gauge Freedom

In this section, we review the electric scalar potential and the magnetic vector potential, and we show to what extent they are related.

Note from (2.6) that we can write the magnetic flux density \mathbf{B} as

$$\mathbf{B} = \nabla \times \mathbf{A} \quad (\text{A.6})$$

Combining the above equation with (2.1) yields

$$\nabla \times (\mathbf{E} + j\omega\mathbf{A}) = 0. \quad (\text{A.7})$$

This equation suggests that the quantity within parentheses can be written as the gradient of some scalar function:

$$\mathbf{E} + j\omega\mathbf{A} = -\nabla\phi, \quad (\text{A.8})$$

or

$$\mathbf{E} = -(\nabla\phi + j\omega\mathbf{A}). \quad (\text{A.9})$$

Here, ϕ is the electric scalar potential, and \mathbf{A} is the magnetic vector potential.

Note that, choosing *any* scalar function ψ , and *any* constant, Equation (A.9) may be manipulated into

$$\mathbf{E} = -[\nabla(\phi - j\omega\psi + \text{const}) + j\omega(\mathbf{A} + \nabla\psi)], \quad (\text{A.10})$$

since when expanding the r.h.s., terms containing ψ cancel, and $\nabla\text{const} = 0$. Comparing again with (A.9), the above equation suggests that we can perform the substitution

$$\begin{aligned} \phi' &\rightarrow \phi - j\omega\psi + \text{const} \\ \mathbf{A}' &\rightarrow \mathbf{A} + \nabla\psi, \end{aligned} \quad (\text{A.11})$$

without affecting the observable quantity \mathbf{E} . The function ψ is called a gauge function, and can be chosen freely to manipulate potential equations into a convenient form.

A.3 The Coulomb gauge

In this section, we review the Coulomb gauge, and show its implications w.r.t. the electric scalar and magnetic vector potential.

Combining (A.4) and (A.9), we obtain

$$\Delta\phi + j\omega\nabla \cdot \mathbf{A} = -\frac{\rho}{\epsilon}. \quad (\text{A.12})$$

Now, in (A.11), we choose ψ such that $\nabla \cdot \mathbf{A}' = 0$. Looking at the second line in (A.11), we see that $\nabla \cdot \mathbf{A} + \Delta\psi = 0$. This equation can be shown to be satisfiable by a function ψ for any \mathbf{A} , and therefore the substitution is sound. Note that, by the substitution we obtain not only a new (primed) version of \mathbf{A} , but also of ϕ . Dropping the primes, we obtain the condition that

$$\nabla \cdot \mathbf{A} = 0, \quad (\text{Coulomb gauge}) \quad (\text{A.13})$$

and (A.12) is transformed into the Poisson equation for the scalar potential

$$\Delta\phi = -\frac{\rho}{\epsilon}. \quad (\text{A.14})$$

Note that the above equation is universally valid (i.e., no assumptions have been made). The simplicity of (A.14) is due to the fact that we used the Coulomb gauge. Also note that the equation has no dependence on the vector potential \mathbf{A} . Unfortunately, using this choice of gauge, the equation for the vector potential becomes somewhat more complicated, as we will show next.

First, plug in (2.3) and (2.4) into (2.2), and combine with (A.6) and (A.9). One then obtains

$$\nabla \times \nabla \times \mathbf{A} + \frac{1}{c^2}(s^2 \mathbf{A} + s \nabla \phi) = \mu \mathbf{J}. \quad (\text{A.15})$$

Using the vector identity (A.23), we get

$$\Delta \mathbf{A} - \frac{s^2}{c^2} \mathbf{A} - \nabla(\nabla \cdot \mathbf{A} + \frac{s^2}{c^2} \phi) = -\mu \mathbf{J} \quad (\text{A.16})$$

Now, using the Coulomb gauge, $\nabla \cdot \mathbf{A} = 0$, we get

$$\Delta \mathbf{A} - \frac{s^2}{c^2} \mathbf{A} = -\mu \mathbf{J} + \frac{s}{c^2} \nabla \phi. \quad (\text{A.17})$$

Note that if we repeat the above derivation, but neglecting the displacement current term, $s\mathbf{D}$, in (2.2), we again obtain an equation of the Poisson form,

$$\Delta \mathbf{A} = \mu \mathbf{J}. \quad (\text{A.18})$$

Note that this equation, however, will not be accurate for high frequencies, since the magnitude of the displacement current term will most likely increase with increasing frequency (note that s will increase linearly with ω , but \mathbf{D} may increase or decrease, depending on the spectral characteristics of the problem at hand; therefore, one cannot simply derive from the above discussion at what frequency the displacement current will become important).

A.4 The Lorenz gauge

In this section, we review the Lorenz gauge. First, combine (A.9) with (2.7) and (2.4). Assume uniform ϵ , and thus write

$$-(\Delta \phi + s \nabla \cdot \mathbf{A}) = \frac{\rho}{\epsilon}. \quad (\text{A.19})$$

Now choose

$$\nabla \cdot \mathbf{A} = -\frac{s}{c^2} \phi, \quad (\text{Lorenz gauge}), \quad (\text{A.20})$$

for a reason that will become clear shortly. Inserting this choice into (A.19), and doing the same with (A.16), we get the equations

$$\Delta \phi - \frac{s^2}{c^2} \phi = -\frac{\rho}{\epsilon}, \quad (\text{A.21})$$

$$\Delta \mathbf{A} - \frac{s^2}{c^2} \mathbf{A} = -\mu \mathbf{J}. \quad (\text{A.22})$$

Thus, we obtain a pair of Helmholtz equations, in which the scalar and vector-potential have essentially a similar role.

A.5 Vector Identities

For reference, this section summarises an important vector-identity. The curl of the curl of a vector-field \mathbf{F} can be written as

$$\nabla \times \nabla \times \mathbf{F} = \nabla \nabla \cdot \mathbf{F} - \Delta \mathbf{F}, \quad (\text{A.23})$$

with

$$\Delta \mathbf{F} \equiv \begin{pmatrix} \Delta F_1 \\ \Delta F_2 \\ \Delta F_3 \end{pmatrix}. \quad (\text{A.24})$$

From this identity, we see that if the vector-field \mathbf{F} is divergence-free, then the curl-curl-operator reduces to the Laplace-operator.

A.6 Green's Theorems

For reference, we recall here the derivation of Green's theorems. Begin with Gauss' law,

$$\int_S \mathbf{f} \cdot d\mathbf{S} = \int_V \nabla \cdot \mathbf{f} dV. \quad (\text{A.25})$$

Plug in $\mathbf{f} = u \nabla v$, to obtain Green's first theorem,

$$\int_S u(dw/dn)dS = \int_V [u\Delta w + \nabla u \cdot \nabla w] dV. \quad (\text{A.26})$$

Interchange u and w , and subtract from (A.26), to obtain Green's second theorem,

$$\int_S [u(dw/dn) - w(du/dn)] dS = \int_V [u\Delta w - w\Delta u] dV. \quad (\text{A.27})$$

Bibliography

- [1] M. Beattie and L. Pileggi. Efficient inductance extraction via windowing. In *DATE '01: Proceedings of Design Automation and Test in Europe*, pages 430–436, March 2001.
- [2] Jarle Berntsen and Terje O. Espelid. Algorithm 706; dcutri: an algorithm for adaptive cubature over a collection of triangles. *ACM Trans. Math. Softw.*, 18(3):329–342, 1992.
- [3] Mike Chou and Jacob White. Multilevel integral equation methods for the extraction of substrate coupling parameters in mixed-signal ic's. In *DAC '98: Proceedings of the 35th annual conference on Design automation*, pages 20–25, San Francisco, California, United States, 1998.
- [4] Joao Paulo Costa, Mike Chou, and L. Miguel Silveira. Efficient techniques for accurate modeling and simulation of substrate coupling in mixed-signal ic's. In *DATE '98: Proceedings of Design Automation and Test in Europe*, pages 892–898, Le Palais des Congres de Paris, France, 1998.
- [5] E. Aykut Dengi and Ronald A. Rohrer. Hierarchical 2-d field solution for capacitance extraction for vlsi interconnect modeling. In *DAC '97: Proceedings of the 34th annual conference on Design automation*, pages 127–132, New York, NY, USA, 1997. ACM Press.
- [6] Ranjit Gharpurey. *Modeling and Analysis of Substrate Coupling in Integrated Circuits*. PhD thesis, University of California, Berkeley, 1995.
- [7] George W. Hanson and Alexander B. Yakovlev. *Operator Theory for Electromagnetics : An Introduction*. Springer-Verlag, New York, 2002.
- [8] H.A. Haus and J.R. Melcher. *Electromagnetic Fields and Energy*. Prentice Hall, Englewood Cliffs, New Jersey, 1989.
- [9] Haitian Hu, David T. Blaauw, Vladimir Zolotov, Kaushik Gala, and Min. Fast on-chip inductance simulation using a precorrected-fft method. *IEEE Transactions on Computer-Aided Design of Integrated Circuits and Systems*, 22:49–66, 2003.
- [10] Daniel Ioan and Catalin Ciobotaru. Equivalent circuits of linear order for electromagnetic field problems. In *Progress in Electromagnetic Research Symposium, PIERS*, Pisa, Italy, 2004.
- [11] J. Kanapka, J. Phillips, and J. White. Fast methods for extraction and sparsification of substrate coupling. In *DAC '00: Proceedings of the 37th annual conference on Design automation*, June 2000.
- [12] Kevin J. Kerns, Ivan L. Wemple, and Andrew T. Yang. Stable and efficient reduction of substrate model networks using congruence transforms. In *ICCAD '95: Proceedings of the International Conference on Computer-aided Design*, pages 207–214, San Jose, California, United States, 1995.

- [13] Simon Kristiansson, Fredrik Ingvarson, Shiva Prasad Kagganti, Nebojsa Simic, Marinel Zgrda, and Kjell O. Jeppson. A surface potential model for predicting substrate noise coupling in integrated circuits. *IEEE Journal of Solid-State Circuits*, 40, September 2005.
- [14] J. R. Phillips and J. White. A precorrected-FFT method for capacitance extraction of complicated 3-D structures. In *ICCAD '94: Proceedings of the Int. Conf. on Computer-Aided Design*, pages 268–271, Santa Clara, California, November 1994.
- [15] P.J. Restle, A.E. Ruehli, S.G. Walker, and G. Papadopoulos. Full-wave peec time-domain method for the modeling of on-chip interconnects. *Computer-Aided Design of Integrated Circuits and Systems, IEEE Transactions on*, 20(7):877–886, 2001.
- [16] A. Ruehli. Inductance calculations in a complex integrated circuit environment. *IBM Journal of Research and Development*, (5):470–481, September 1972.
- [17] J. M. S. Silva and L. Miguel Silveira. Multigrid-based substrate coupling model extraction. In *ISCAS '04: Proceedings of the International Symposium on Circuits and Systems*, volume 5, pages 169–173, May 2004.
- [18] T. Smedes, N. P. van der Meijs, and A.J. van Genderen. Boundary element methods for capacitance and substrate resistance calculations in a vlsi layout verification package. In *Proc. International Conf. on Software for Elect. Eng. Analysis and Design*, pages 337–344, July 1993.
- [19] Ivar Stakgold. *Boundary value problems of mathematical physics (vol. 2)*. Society for Industrial and Applied Mathematics, Philadelphia, PA, USA, 2000.
- [20] O. Steinbach and W.L. Wendland. The construction of some efficient preconditioners in the boundary element method. *Advances in Computational Mathematics*, 9(1-2):191–216, September 1998.
- [21] G. Veronis, Y.-C. Lu, and R. W. Dutton. Modeling of wave behavior of substrate noise coupling for mixed-signal ic design. In *ISQED '04: Proc. of the IEEE International Symposium on Quality Electronic Design*, pages 303–308, San Jose, CA, USA, April 2004.
- [22] Georgios Veronis, Yi-Chang Lu, and Robert W. Dutton. Modeling of wave behavior of substrate noise coupling for mixed-signal ic design. In *ISQED '04: Proceedings of the 5th International Symposium on Quality Electronic Design*, pages 303–308, Washington, DC, USA, 2004. IEEE Computer Society.
- [23] Junfeng Wang. *A new surface integral formulation of EMQS impedance extraction for 3-D structures*. PhD thesis, MIT, EECS Department, September 1999.
- [24] J. White, J. Phillips, and T. Korsmeyer. Comparing precorrected fft and fast multipole algorithms for solving three dimensional potential problems. In *Proceedings of the Colorado Conference on Iterative Methods*, Breckenridge, Colorado, April 1994.

- [25] D. Wilton, S. Rao, A. Glisson, D. Schaubert, O. Al-Bundak, and C. Butler. Potential integrals for uniform and linear source distributions on polygonal and polyhedral domains. *IEEE Transactions on Antennas and Propagation*, 32(3):276–281, March 1984.
- [26] H. Yu and L. He. Vector potential equivalent circuit based on peec inversion. Technical report, University of California, 2003.
- [27] Zhenhai Zhu, Jingfang Huang, Ben Song, and Jacob White. Improving the robustness of a surface integral formulation for wideband impedance extraction of 3d structures. In *ICCAD '01: Proceedings of the Int. Conf. on Computer-Aided Design*, pages 592–597, Piscataway, NJ, USA, 2001. IEEE Press.